universe

MDPI

Article

Bound Orbits and Epicyclic Motions around Renormalization Group Improved Schwarzschild Black Holes

Hou-Yu Lin [1,2] and Xue-Mei Deng [1,*]

[1] Purple Mountain Observatory, Chinese Academy of Sciences, Nanjing 210033, China; linhy@pmo.ac.cn
[2] School of Astronomy and Space Science, University of Science and Technology of China, Hefei 230026, China
* Correspondence: xmd@pmo.ac.cn

Abstract: We study timelike particles' bound orbits around renormalization group improved Schwarzschild black holes (RGISBHs), which originate from renormalization group improvement of the Einstein–Hilbert action by using the running Newton constant. By considering the secular periastron precession for the timelike particles orbiting around RGISBHs, we found that it is not feasible to distinguish such black holes from Schwarzschild ones in the weak gravitational field. However, in the strong gravitational field, periodic orbits for the particles are investigated by employing a taxonomy. This suggests that the variation of the parameters in RGISBHs can change the taxonomy. This leads to a transition from periodic motion around Schwarzschild black holes to a quasi-periodic motion around these black holes. After that, the epicyclic motions of charged particles around RGISBHs immersed in an external asymptotically uniform magnetic field are taken into account with respect to the observed twin peak quasi-periodic oscillations' frequencies. The epicyclic motions of charged particles around such black holes in the external magnetic field can give one possible explanation for the 3:2 resonance in three low-mass X-ray binaries. Our results might provide some hints to distinguish RGISBHs from the classical black holes by using periodic orbits and epicyclic motions around the strong gravitational field.

Keywords: gravitation; general relativity; alternative theories of gravity; astrometry

Citation: Lin, H.-Y.; Deng, X.-M. Bound Orbits and Epicyclic Motions around Renormalization Group Improved Schwarzschild Black Holes. *Universe* **2022**, *8*, 278. https://doi.org/10.3390/universe8050278

Academic Editor: Lorenzo Iorio

Received: 7 April 2022
Accepted: 8 May 2022
Published: 10 May 2022

1. Introduction

Black holes are fundamental objects predicted by Einstein's general relativity (GR). The detection of gravitational waves from binary black holes [1–6], X-ray binaries such as Cygnus X-1 (see [7–9] and the references therein), and imaging the supermassive black hole at the center of the giant elliptical galaxy M87 [10–15] not only uncover that black holes are plentiful in our Universe, but also open new ways to explore some influences of new physics on the strong gravitational fields [16–46]. One key feature that makes an object a black hole in GR is the existence of the event horizon around a central spacetime singularity. However, the event horizon causes the information paradox and the problem of the black hole singularity implies that GR should be improved. Now, it is commonly believed that one kind of the self-consistent quantum gravity can erase these flaws in GR due to high energy density and exceeding curvature in quantum gravity (see [47] for details).

Some effects of quantum gravity on black holes have been widely investigated, which include the Hawking evaporation process [48–50], entanglement [51–54], and the information loss paradox [55–58]. Some modified theories based on quantum gravity have been developed by Koch and collaborators (Rioseco and Rincón) [59–70]. They developed an alternative approach based on quantum gravity where the coupling constants can vary. It is remarkable that some quantum gravity effects can resolve the singularity of black holes by using the renormalization group improvement approach [71,72]. This leads to renormalization group improved Schwarzschild black holes (RGISBHs), proposed by Bonanno and Reuter [71]. RGISBHs originate from renormalization group improvement

of the Einstein–Hilbert action by using the running Newton constant, borrowed from a standard scheme in particle physics. Some interesting properties for RGISBHs had be well studied in the regularity and thermodynamics [71], the quantum gravitational effects on accretion [73], the strong deflection lensing [74], as well as the dynamics of test particles around the black holes [75], whereas bound (precessing/periodic) orbits and epicyclic motions around RGISBHs are still missing in the literature.

Precessing and periodic orbits belong to two particular subclasses of the bound orbits and play a very important role in testing modified gravity theories. For example, the perihelion shifts of the planets in the Solar System [76–84], of exoplanets [85–88], of binary pulsars [89–94], and of stars around SgrA* [95–98] have widely been used to constrain GR and modified gravity theories. These precessing orbits in the weak gravitational field are very similar to the one of Mercury's perihelion precession. When a timelike particle is near a black hole, however, the bound orbits reveal the zoom-whirl quasi-periodic and periodic motions, and this belongs to a unique feature in the strong gravitational field [99–102]. Following [103], one rational number q can be used to describe this zoom-whirl behavior for the timelike particle's motion close to a black hole. These bound orbits with q have been extensively investigated in some classical black holes in GR [103,104] and other black holes in modified gravity theories [21,105–115]. Therefore, precessing and periodic orbits are mainly considered in the present work.

In addition, epicyclic motions around RGISBHs are also investigated in this paper. Recently, quasi-periodic oscillations (QPOs) are recognized as promising ways to detect some quantum effects and to measure possible deviations from GR in the strong gravitational field [116–128]. QPOs have been observed and identified under three microquasars in our galaxy: GRS 1915+105, XTE 1550-564, and GRO 1655-40. In this astrophysical system, one can observe the twin high-frequency QPOs with the perfect 3:2 frequency ratio. Up to now, there is still no consensus on which physical mechanism is responsible for the twin high-frequency QPOs. However, these frequencies are correlated with the orbital characteristic frequencies of a test particle (see [8,9] for reviews). Since these epicyclic motions are only determined by the metric and are independent of the complicated astrophysical processes of the accretion, they might present an opportunity to test modified gravity theories.

In Section 2, we briefly review the metric for RGISBHs and give the geodesics of the timelike particles around the black holes. In Section 3, we study the bound orbits around RGISBHs for the timelike particles. In the upcoming sections, we mainly pay attention to the effects of RGISBHs on bounds orbits and epicyclic motions. In Section 4, we deliberate about the precessing and periodic orbits around RGISBHs. In Section 5, we investigate the epicyclic motions of charged particles around RGISBHs immersed in an external asymptotically uniform magnetic field. In Section 6, we give the conclusions and discussion of the present work.

2. Metric and Geodesics

Some quantum effects in one Schwarzschild spacetime are usually incorporated by using the approach of the renormalization group (RG), where Newton's gravitational constant varies with a length scale. Inspired by these ideas, Bonanno and Reuter investigated the impact of the leading quantum gravity effects on the dynamics of the Hawking evaporation process of a black hole [71]. The spacetime metric of the black hole is represented by an RG improved Vaidya one and is called the renormalization group improved Schwarzschild Black holes (RGISBHs). If the mass of such a black hole [71] reaches a critical one, the RGIBH evaporation terminates. The final state of the evaporation process is a cold, Planck size remnant (see [71] for details). The spacetime of RGISBHs [71] is

$$\mathrm{d}s^2 = -f(r)\mathrm{d}t^2 + \frac{1}{f(r)}\mathrm{d}r^2 + r^2(\mathrm{d}\theta^2 + \sin^2\theta\mathrm{d}\phi^2), \tag{1}$$

where

$$f(r) = 1 - \frac{2GM}{c^2 r}\left(1 + \frac{\tilde{\omega} G\hbar}{c^3 r^2} + \gamma \frac{\tilde{\omega} G\hbar M}{c^5 r^3}\right)^{-1}, \tag{2}$$

in which $\tilde{\omega}$ comes from the theory of nonperturbative renormalization groups and γ is the identification of the cutoff for the distance scale [71]. These two parameters are all dimensionless. When $\tilde{\omega} = \gamma = 0$, the metric (1) will reduce to the Schwarzschild one.

Following the work of [74], we adopt $G = c = \hbar = 1$ in the following work, and the dimensionless function (2) yields

$$f(r) = 1 - \frac{2M}{r}\left(1 + \Omega \frac{M^2}{r^2} + \gamma \Omega \frac{M^3}{r^3}\right)^{-1}, \tag{3}$$

by taking $\Omega \equiv \tilde{\omega}/M^2$. The event horizons for RGISBHs can be derived from $g^{rr} = 0$, which is equal to $f(r) = 0$. One can find that there exits no, single, or double horizons for RGISBHs. The discriminant for $f(r) = 0$ is described as in [74]:

$$\Delta_3 = -M^6 \Omega(\Omega - \Omega_+)(\Omega - \Omega_-), \tag{4}$$

with

$$\Omega_\pm = -\frac{27}{8}\gamma^2 - \frac{9}{2}\gamma + \frac{1}{2} \pm \frac{1}{8}\sqrt{(\gamma + 2)(9\gamma + 2)^3}, \tag{5}$$

where the cubic equation has no or double positive roots only when $\Omega > 0$ and $\gamma > 0$. If the discriminant Δ_3 is greater than zero, we must have $\Omega < \Omega_+$ due to $\Omega_- < 0$. Then, a new dimensionless parameter λ is introduced as follows [74]:

$$\lambda = \frac{\Omega}{\Omega_+} \in (0, 1]. \tag{6}$$

For $0 < \lambda < 1$, there exist two event horizons: the internal and external one. When $\lambda = 1$, the two horizons shrink into a single one. Otherwise, no horizon can survive. Figure 1 shows the metric $f(r)$ as a function of r/M with various values of λ and γ. It is worth noting that destroying the event horizon can violate the area theorem [129], which can lead to the energy released in the collision of two black holes exceeding the Hawking radiation. Since this violation is not supported by the current observations of gravitational waves, we only consider the case for $0 < \lambda \leq 1$ in the present work.

In $\theta = \pi/2$, the Lagrangian for a test particle yields

$$2\mathcal{L} = -f(r)\dot{t}^2 + \frac{1}{f(r)}\dot{r}^2 + r^2\dot{\phi}^2, \tag{7}$$

in which a dot denotes a derivative with respect to one affine parameter. We have

$$P_t = \frac{\partial \mathcal{L}}{\partial \dot{t}} = -f(r)\dot{t} = -E, \tag{8}$$

$$P_r = \frac{\partial \mathcal{L}}{\partial \dot{r}} = \frac{1}{f(r)}\dot{r}, \tag{9}$$

$$P_\phi = \frac{\partial \mathcal{L}}{\partial \dot{\phi}} = r^2\dot{\phi} = L, \tag{10}$$

where E and L are the particle's conserved energy and angular momentum. The Hamiltonian $\mathcal{H}$ for the test particle is

$$\mathcal{H} = P_t\dot{t} + P_\phi\dot{\phi} + P_r\dot{r} - \mathcal{L}. \tag{11}$$

Then, we derive the following form:

$$2\mathcal{H} = -E\dot{t} + \frac{1}{f(r)}\dot{r}^2 + L\dot{\phi} = \delta. \tag{12}$$

The equation of motion for the test particle can be written as

$$\dot{r}^2 = f(r)\left(\delta - \frac{L^2}{r^2} + \frac{E^2}{f(r)}\right), \tag{13}$$

by substituting Equations (8)–(10) into Equation (12). In the above equations, $\delta = -1$ for the timelike particles. The effective potential for one timelike particle is defined as [130]

$$\begin{aligned} V_{\rm eff} &\equiv E^2 - \dot{r}^2 \\ &= \left[1 - \frac{2M}{r}\left(1 + \Omega\frac{M^2}{r^2} + \gamma\Omega\frac{M^3}{r^3}\right)^{-1}\right]\left(1 + \frac{L^2}{r^2}\right). \end{aligned} \tag{14}$$

In Equation (14), $\Omega = \lambda\Omega_+ = \lambda[-27\gamma^2/8 - 9\gamma/2 + 1/2 + \sqrt{(\gamma+2)(9\gamma+2)^3}/8]$ based on Equation (6). It is shown that the effective potential mainly depends on r, L, and the parameters of λ and γ. By using Equation (14), the bound orbits around RGISBHs will be investigated in the next section.

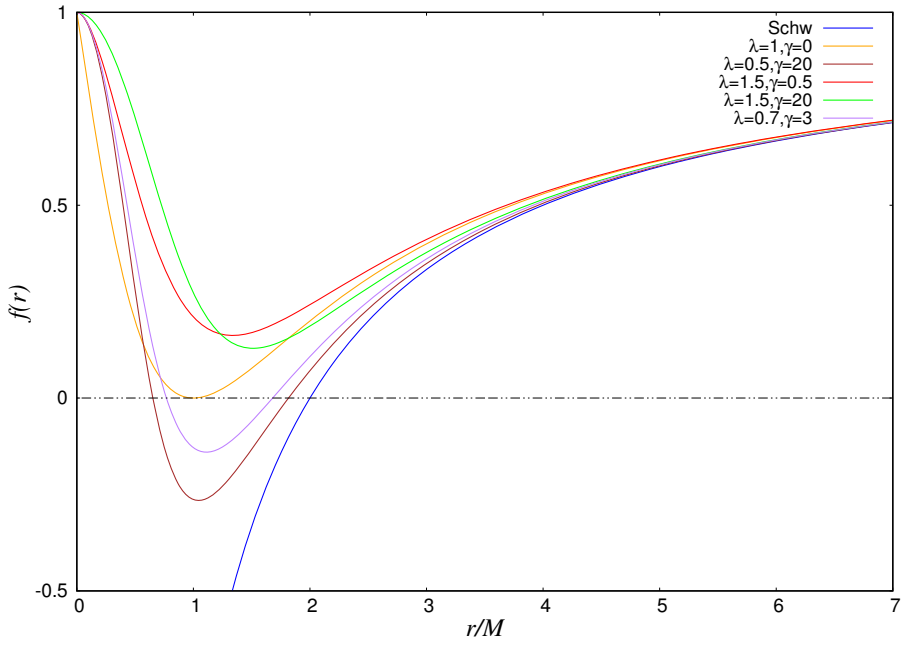

Figure 1. $f(r)$ as a function of r/M.

3. Bound Orbits

For the timelike particle around RGISBHs, the bound orbits are located between the marginally bound orbits (MBOs) and the innermost stable circular orbits (ISCOs), which are derived from Equation (14). MBOs for the particle around RGISBHs should satisfy the following conditions [131]:

$$V_{\rm eff} = 1, \quad \partial_r V_{\rm eff} = 0, \tag{15}$$

which belong to an unstable circular orbits. For ISCOs, it reads [131]

$$V_{\rm eff} = E^2, \quad \partial_r V_{\rm eff} = 0, \quad \partial_r\partial_r V_{\rm eff} = 0. \tag{16}$$

which is a minimal radius permitting the stable circular orbit for the particle around RGISBHs.

Figure 2 indicates $r_{\rm MBO}/M$ and $L_{\rm MBO}/M$ of the timelike particle around RGISBHs with respect to λ and γ for MBOs. It suggests that, in some cases (e.g., $0.25 < \lambda < 1$), the values of $r_{\rm MBO}/M$ and $L_{\rm MBO}/M$ in RGISBHs are smaller than the values in Schwarzschild black holes. In the classical Schwarzschild case, $r_{\rm MBO}/M = 4$ and $L_{\rm MBO}/M = 4$. Figure 3 displays $r_{\rm ISCO}/M$, $L_{\rm ISCO}/M$, and $E_{\rm ISCO}$ of the timelike particle around RGISBHs with respect to λ and γ for ISCOs. Furthermore, in some cases, the values of $r_{\rm ISCO}/M$, $L_{\rm ISCO}/M$, and $E_{\rm ISCO}$ are smaller than the ones in Schwarzschild black holes. In the Schwarzschild case, $r_{\rm ISCO}/M = 6$, $E_{\rm ISCO} = 2\sqrt{2}/3$, and $L_{\rm ISCO}/M = 2\sqrt{3}$. This means that the energy and angular momentum of the bound orbits around RGISBHs might be smaller than the classical Schwarzschild one.

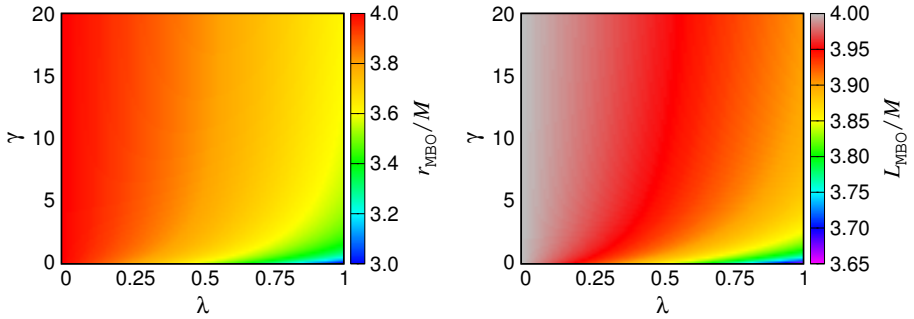

Figure 2. $r_{\rm MBO}/M$ and $L_{\rm MBO}/M$ of a timelike particle around RGISBHs with respect to λ and γ.

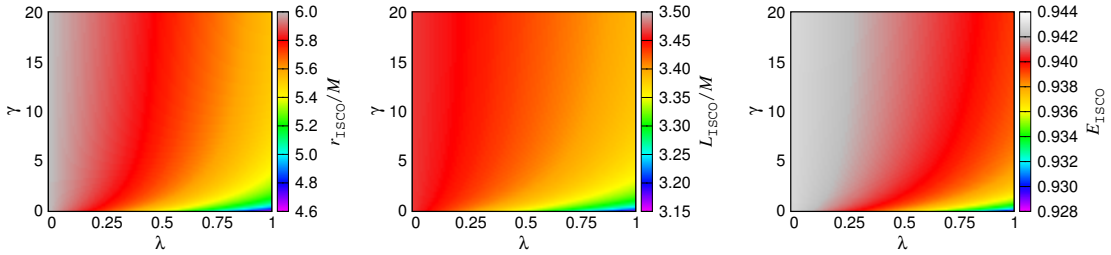

Figure 3. $r_{\rm ISCO}/M$, $L_{\rm ISCO}/M$, and $E_{\rm ISCO}$ of a timelike particle around RGISBHs with respect to λ and γ.

The effective potential $V_{\rm eff}$ as a function of r/M is plotted in Figure 4 with different values of L/M, λ, and γ. The angular momentum varies from $L_{\rm MBO}/M$ to $L_{\rm ISCO}/M$ from top to bottom in Figure 4. From Figure 4, it shows that, when the angular momentum increases, the values of $V_{\rm eff}$ become large until the angular momentum reaches $L_{\rm MBO}/M$. Besides, the effective potential with $L_{\rm ISCO}/M$ has only one extremal point, and other cases have two extremal points in Figure 4. For a given L/M, it also suggests that E cannot be too high, otherwise the particle falls into the black hole, and E cannot be too small, otherwise there is no solution. This enables one to plot the allowed $(L/M, E)$ regions for the bound orbits (in shadow) around RGISBHs with various values of λ and γ, as shown in Figure 5. This figure indicates that $E_{\rm min} \leq E \leq E_{\rm max}$ for a fixed L/M. All of the values for $E_{\rm min}$ form the blue curves in Figure 5, while the red curves consist of all values for $E_{\rm max}$.

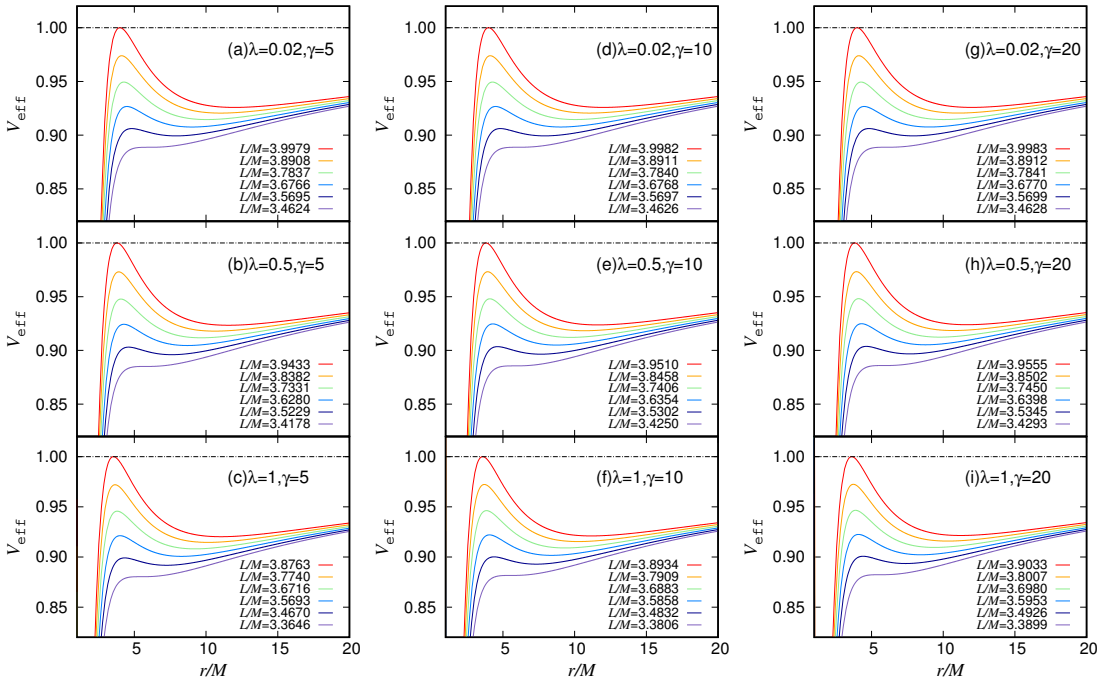

Figure 4. The effective potential $V_{\rm eff}$ as a function of r/M with different values of L/M, λ, and γ. The angular momentum varies from $L_{\rm MBO}/M$ to $L_{\rm ISCO}/M$ from top to bottom.

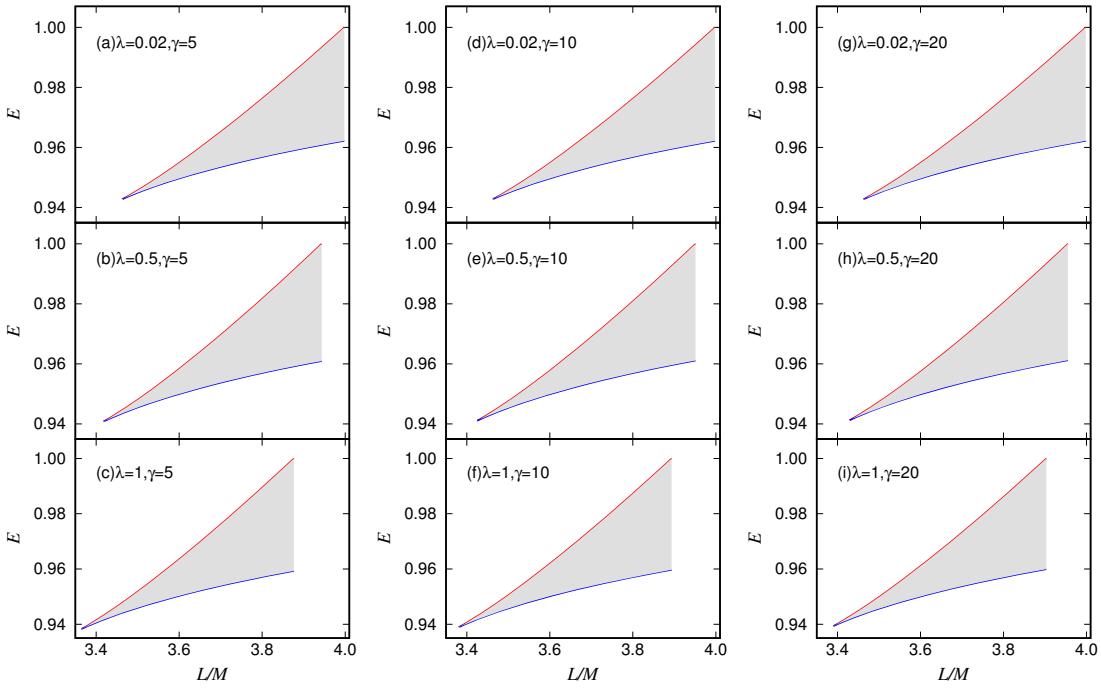

Figure 5. $(L/M, E)$ regions for the bound orbits (in shadow) around RGISBHs with various values of λ and γ. The red and the blue curves are the upper and the lower bounds for E, respectively.

It should be emphasized that [75] investigated the dynamics of neutral, electrically charged, and magnetized particles around RGIBHs in the presence of an external asymptotically uniform magnetic field. These bound orbits around RGISBHs have been partly considered by previous work [75]. The differences between [75] and the present work are as follows: (i) The marginally bound orbits (MBOs) are considered in the present work. In [75], only the marginally and the innermost stable circular orbits (MSCOs and ICSOs)

were considered. The MBOs are very useful for the analysis of the bound orbits and the following precessing and periodic orbits. In fact, for MBOs, one test massive particle has the same energy $E = 1$ as the particle at rest at infinity. This also means that there is no dissipation of energy when the massive particle is transferred from infinity to the MBO. If its motion is far beyond the MBO, the particle can completely escape from the gravitational field of the black hole. (ii) ISCOs are displayed by various parameters γ and λ (Figure 2) in this paper. In [75], only specific parameter values such as a fixed value $\lambda = 1$ were considered (see Figure 4 in [75]). (iii) The effective potential $V_{\rm eff}$ as a function of r/M is studied in the present paper. (iv) $(L/M, E)$ regions for the bound orbits around RGISBHs are also taken into account in our work. These characteristics of (i)–(iv) in our work are devoted to investigating precessing and periodic orbits.

By taking a fixed L/M, E, and the parameters of λ and γ, an irrational or a rational number q [103] could represent each of bound orbit around RGISBHs. q can describe the amount of the precession of the orbit in one radial cycle from one apastron to periastron to the next apastron; it reads [103]

$$\Delta\phi = 2\pi(q+1), \tag{17}$$

where a rational number denotes one periodic orbit and an irrational number denotes a precessing or quasi-periodic one (see [103] for details). They all belong to the bound orbits. Then, we derive

$$\Delta\omega \equiv \Delta\phi - 2\pi = 2\pi q. \tag{18}$$

The corresponding rational number q is decomposed into three integers (z, w, ν) [103] as follows:

$$q = w + \frac{\nu}{z}, \tag{19}$$

where z is the "zoom" number and w is the "whirl" number. ν denotes the "vertices" number formed by joining the successive apastron of the periodic orbit. The equatorial angle reads

$$\Delta\phi = \oint \mathrm{d}\phi. \tag{20}$$

Equation (20) can be rewritten as

$$\Delta\phi = 2\int_{r_{\rm pe}}^{r_{\rm ap}} \frac{\mathrm{d}\phi}{\mathrm{d}r}\mathrm{d}r = 2\int_0^{\pi} \frac{\mathrm{d}\phi}{\mathrm{d}\chi}\mathrm{d}\chi, \tag{21}$$

where $r_{\rm pe}$ and $r_{\rm ap}$ denote periastron and apastron, respectively. We can parameterize the orbit as

$$r = \frac{a(1-e^2)}{1+e\cos\chi}, \tag{22}$$

in which a is the semimajor axis and e is the eccentricity. When $\chi = 0$ and $\chi = \pi$, the periastron and apastron based on Equation (22) can be expressed as follows:

$$r_{\rm pe} = a(1-e), \quad r_{\rm ap} = r(1+e). \tag{23}$$

From Equations (10), (13), and (22), we have

$$\frac{\mathrm{d}\phi}{\mathrm{d}\chi} = \frac{ae(1-e^2)L\sin\chi}{r^2(1+e\cos\chi)^2\sqrt{E^2 - f(r)\left(1+\frac{L^2}{r^2}\right)}}, \tag{24}$$

with

$$L^2 = \frac{r_{\rm ap}^2 r_{\rm pe}^2 [f(r_{\rm pe}) - f(r_{\rm ap})]}{r_{\rm pe}^2 f(r_{\rm ap}) - r_{\rm ap}^2 f(r_{\rm pe})}, \tag{25}$$

$$E^2 = \frac{f(r_{\rm ap}) f(r_{\rm pe})(r_{\rm pe}^2 - r_{\rm ap}^2)}{r_{\rm pe}^2 f(r_{\rm ap}) - r_{\rm ap}^2 f(r_{\rm pe})}, \tag{26}$$

where L and E are obtained from $\dot{r}|_{r=r_{\rm ap}} = 0$ and $\dot{r}|_{r=r_{\rm pe}} = 0$. In the next section, we will study precessing and periodic orbits around RGISBHs by using the above expressions.

4. Precessing and Periodic Orbits

Precessing motion belongs to one kind of specific class for the bound orbit with an irrational number q. Recently, GRAVITY reported the first detection of GR's Schwarzschild precession in the orbit of the S2 star around Sgr A* [96]. The observation by GRAVITY confirms that the inferred precession $\Delta\omega_{\rm S2}$ as the Schwarzschild one $\Delta\omega_{\rm GR}$ is [96]

$$f_{\rm SP} \equiv \frac{\Delta\omega_{\rm S2}}{\Delta\omega_{\rm GR}} = 1.10, \tag{27}$$

where the Schwarzschild precession in the second post-Newtonian (2PN) approximation having the following form [132]:

$$\Delta\omega_{\rm GR} = \frac{6\pi M_\bullet}{a(1-e^2)} + \frac{3\pi(18+e^2)M_\bullet^2}{2(1-e^2)^2 a^2} + \mathcal{O}(M_\bullet^3). \tag{28}$$

If RGISBHs are the candidate for the supermassive black hole at the Galactic Center, the S2 star' precession is derived as

$$\begin{aligned} \Delta\omega_{\rm RGI} &= \Delta\phi - 2\pi = 2\int_0^\pi \frac{{\rm d}\phi}{{\rm d}\chi}{\rm d}\chi - 2\pi \\ &= \frac{6\pi M_\bullet}{a(1-e^2)} + \frac{3\pi(18+e^2-4\Omega)M_\bullet^2}{2(1-e^2)^2 a^2} + \mathcal{O}(M_\bullet^3), \end{aligned} \tag{29}$$

at the 2PN level. $\Omega = \lambda\Omega_+ = \lambda[-27\gamma^2/8 - 9\gamma/2 + 1/2 + \sqrt{(\gamma+2)(9\gamma+2)^3}/8]$ based on Equation (6). Then, Equation (27) is represented as

$$f_{\rm SP} \equiv \frac{\Delta\omega_{\rm RGI}}{\Delta\omega_{\rm GR}} = 1.10. \tag{30}$$

By using the data of the orbit for the S2 star around Sgr A* in GRAVITY [96], we can plot the precessing $f_{\rm SP}$ in the weak gravitational field (see Figure 6). Here, the bound on the parameters as $0.02 \leq \lambda \leq 0.22$ and $0.2 \leq \gamma \leq 20$ under RGISBHs was given by [74], which is constrained by making use of the data for the shadow of the M87 central black hole. In Figure 6, at this bound on λ and γ, it indicates that the precessing in RGISBHs might be either positive or negative. However, one negative precession is not supported by any available observations. Therefore, this rules out the parameters range of λ and γ, e.g., $0.144 \leq \lambda \leq 0.22$ when $0.2 \leq \gamma \leq 0.3$, with the negative precession. Based on the observation of GRAVITY, $f_{\rm SP} = 1.1$, which is labeled in Figure 6. This leads to $0.6 \leq \gamma \leq 1.02$ when $0.02 \leq \lambda \leq 0.22$. This also means that it is not feasible to distinguish such black holes from classical Schwarzschild ones in the weak gravitational field.

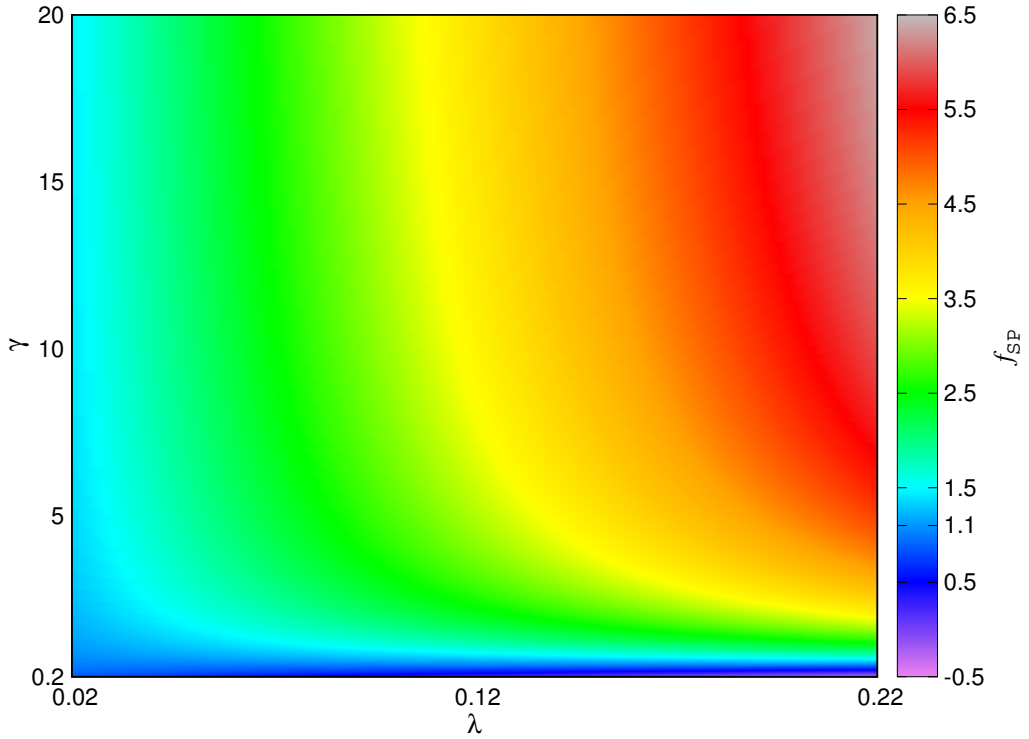

Figure 6. Precessing of the S2 star around RGISBHs f_{SP} in the weak gravitational field with $0.02 \leq \lambda \leq 0.22$ and $0.2 \leq \gamma \leq 20$.

In the strong gravitational field, a rational number q in Equation (19) can describe one periodic orbit, which also belongs to one particular subclass of the bound orbits. Based on Equations (17)–(21), q is determined by $\Delta\phi$ and $\Delta\phi$ depends on the metric (2), the angular momentum L, and the energy E. Figure 7 displays q versus E (the left panel) and q versus L/M (the right panel) with different values of λ and γ. In the right panel in this figure, it is indicated that the increment of L/M can decrease the value of q. In the left panel of this figure, the increment of E can increase the value of q. From Figure 7, we can see that q is more sensitive to the parameter γ in comparison to the parameter λ. The variations in the values of γ make the difference between these curves.

Figure 8 indicates periodic and quasi-periodic orbits around RGISBHs with $L/M = 3.8$. Each column in Figure 8 has the same values of λ and γ, while each row shares the same value of E. In this figure, the classical Schwarzschild black holes (denoted by "Schw") display perfect periodic orbits with three integers (z, w, ν) and the relevant rational number q. In other situations, the values of q under RGISBHs belong to quasi-periodic orbits by taking the same value of E as the one in the Schwarzschild case.

In each row of Figure 8, with the same values of E and L/M, the change of λ and γ makes the particles around RGISBHs have quasi-periodic orbits in spite of the periodic orbits in the Schwarzschild case. The behaviors of quasi-periodic orbits are quite different in each row. For example, in the first row, the timelike particle around Schwarzschild black holes has the periodic orbit with $q = 1$. With the same values of E and L/M in the row, the quasi-periodic orbit with $\lambda = 0.5$ and $\gamma = 10$ has $q \approx 0.797935$. This quasi-periodic orbit approaches the periodic one with $q = 4/5$ and is quite different from $q = 1$. Another case is the quasi-periodic orbit in the last row with $\lambda = 0.02$ and $\gamma = 0.2$ with $q \approx 1.429947$. This situation is very close to the periodic orbit of $q = 1 + 1/2$ and is also different from $q = 2$ for the classical Schwarzschild case. Due to the bound orbits in the strong gravitational field, we might be able to distinguish RGISBHs from the classical Schwarzschild black holes. For example, in the near future observations, if GRAVITY can find S stars nearby Sgr A* and report these precessions in the orbit around Sgr A* with the high-precision, quasi-periodic orbits around RGISBHs will be detectable. However, these observations

must be modeled under RGISBHs firstly, and the parameters λ and γ will be obtained by fitting data.

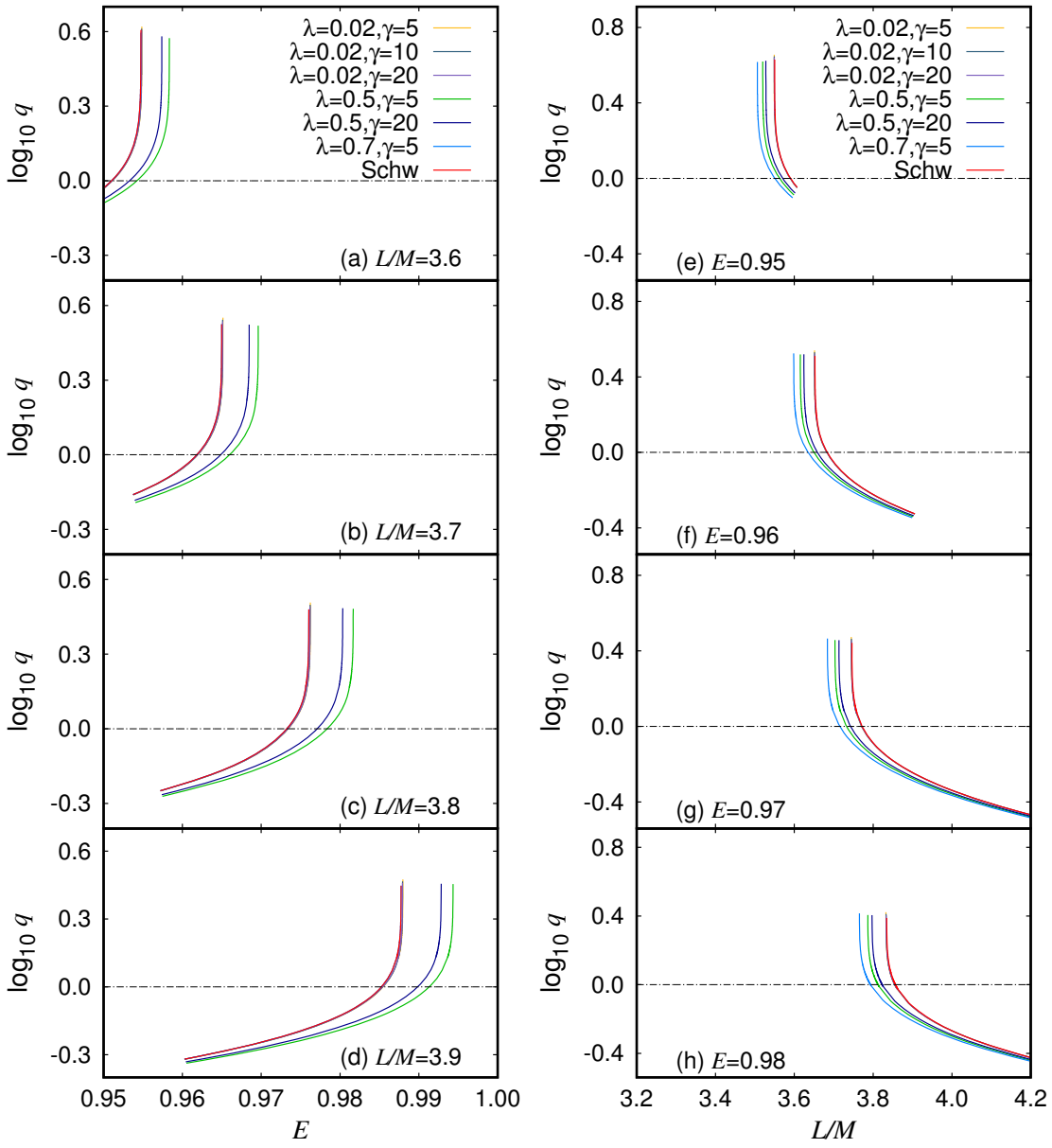

Figure 7. q versus E (left panel) and q versus L/M (right panel) with different parameters values.

In summary, for the quasi-periodic and periodic orbits with the same values of L/M and E around RGISBHs, it is indicated that: (1) the variations in the values of λ and γ make a transition from one periodic orbit to one quasi-periodic one and vice versa; (2) the behaviors of quasi-periodic orbits are quite different with the change of the parameters λ and γ; (3) the bound orbits around RGISBHs in the strong gravitational field are quite different from the Schwarzschild ones.

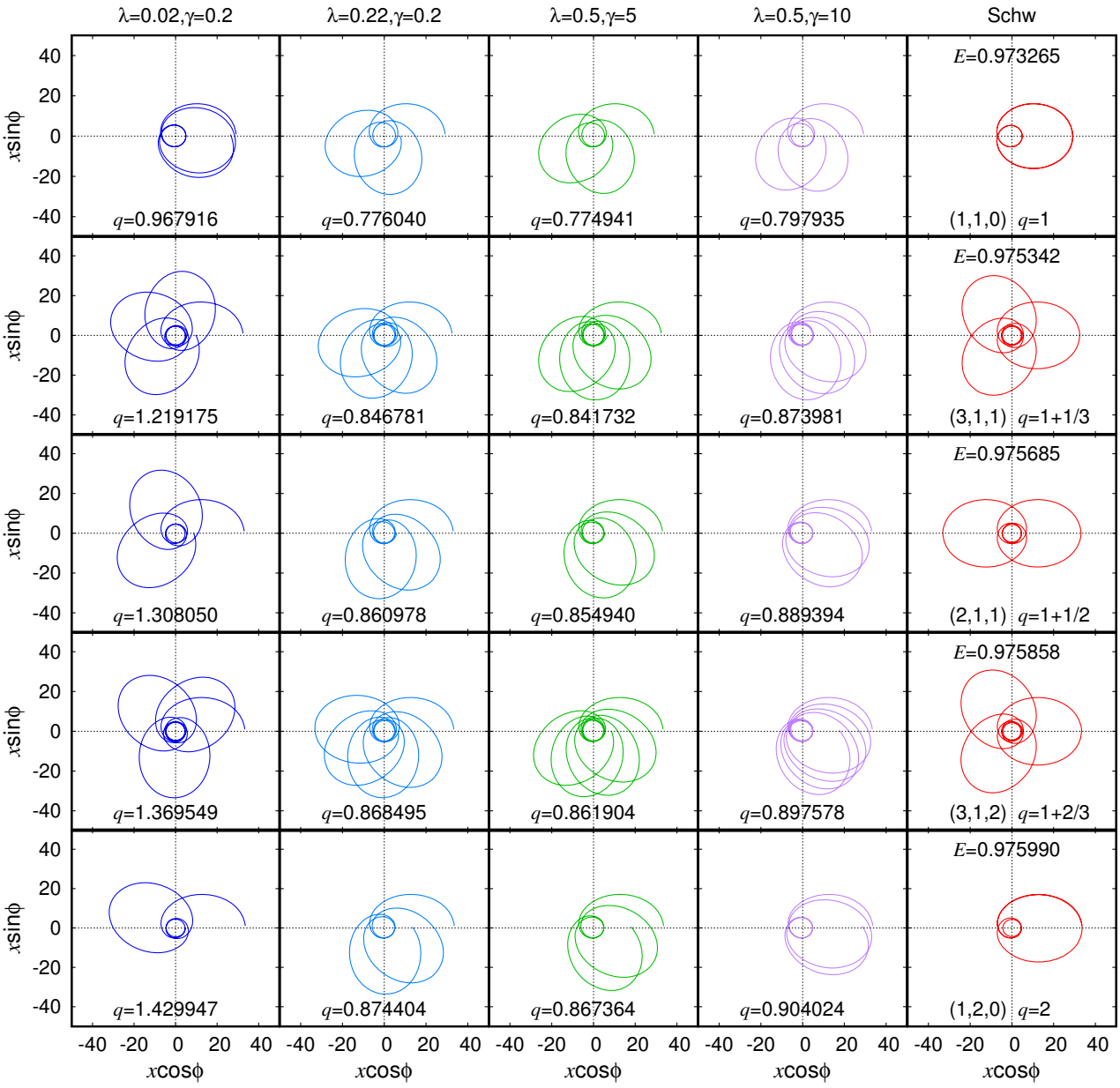

Figure 8. The quasi-periodic and periodic orbits around RGISBHs with $L/M = 3.8$. Each column has the same values of λ and γ, while each row shares the same value of E.

5. Epicyclic Motions and Mass-Limit of Microquasars

In the astrophysics cases, one external magnetic field can exist around one black hole with an accretion disk. This can affect the charged particle's motion around the black hole. Much work has widely considered the charged test particles' motions around black holes surrounded by an external magnetic field [75,133–139] and the chaotic behaviors and the relevant integrators [140–148]. In [75], the dynamics of the charged particles around RGISBHs immersed in an external asymptotically uniform magnetic field was considered. We first briefly review the dynamics of the charged particles around RGISBHs for completeness (see [75] for details). Then, the epicyclic motions of charged particles around RGISBHs in the external magnetic field will be modeled and compared with the observations for microquasars.

In their work [75], the external asymptotically uniform magnetic field B_0 is perpendicular to the equatorial plane $\theta = \pi/2$ by using the method of Wald in [133]. In [133], Wald pioneered and derived the solution for the electromagnetic field occurring when one

axisymmetric, stationary black hole is put in one uniform magnetic field aligned along the symmetry axis of the black hole. In this method [133], one Killing vector serves as a vector potential for a Maxwell field (see [133] for details). Then, A_μ can be written as the following forms:

$$A_\phi = \frac{1}{2}B_0 r^2 \sin^2\theta, \tag{31}$$
$$A_t = A_r = A_\theta = 0, \tag{32}$$

and the following nonzero components in $F_{\mu\nu} \equiv A_{\nu,\mu} - A_{\mu,\nu}$ are

$$F_{r\phi} = B_0 r \sin^2\theta, \tag{33}$$
$$F_{\theta\phi} = B_0 r^2 \sin\theta\cos\theta. \tag{34}$$

For a proper observer, the orthonormal component of the asymptotically uniform magnetic field around RGISBHs yields

$$B^\alpha = \frac{1}{2}\eta^{\alpha\beta\delta\lambda}F_{\beta\delta}u_\lambda, \tag{35}$$

in which $\eta_{\alpha\beta\delta\lambda}$ is the pseudotensorial form of the Levi-Civita symbol and u_λ is the four-velocity for the proper observer [131]. This leads to

$$B^{\hat{r}} = B_0\cos\theta, \quad B^{\hat{\theta}} = \sqrt{f(r)}B_0\sin\theta. \tag{36}$$

The Hamilton–Jacobi equation for RGISBHs [131] is

$$g^{\mu\nu}\left(\frac{\partial S}{\partial r^\mu} - qA_\mu\right)\left(\frac{\partial S}{\partial r^\nu} - qA_\nu\right) = -m^2, \tag{37}$$

where m and q denote, respectively, the particle's mass and electric charge. The corresponding action reads

$$S = -Et + L\phi + S_r(r) + S_\theta(\theta). \tag{38}$$

It yields

$$\dot{t} = \frac{E}{f(r)}, \tag{39}$$
$$\dot{\phi} = \frac{L}{r^2\sin^2\theta} - \frac{1}{2}b, \tag{40}$$
$$\frac{1}{f(r)}\dot{r}^2 + r^2\dot{\theta}^2 = -2U(r,\theta,E,L,b), \tag{41}$$

with

$$U(r,\theta,E,L,b) = -\frac{E^2}{2f(r)} + \frac{1}{2}\left(\frac{L}{r\sin\theta} - \frac{1}{2}br\sin\theta\right)^2 + \frac{1}{2}, \tag{42}$$

where $b = qB_0/m$. This parameter is called the cyclotron frequency as a result of the Lorenz force and represents the interaction between the magnetic field and the charged particle. In Equation (42), L can be positive or negative. When $L/M > 0$ and $b > 0$ (or $L/M < 0$ and $b < 0$), the Lorentz force is repulsive. While $L/M < 0$ and $b > 0$ (or $L/M > 0$ and $b < 0$), the Lorentz force is attractive. This enables the charged particle to have three qualitatively different types of trajectories (see [134] for details).

One microquasar in our galaxy has been identified as a stellar mass black hole, which has an accretion disk. This microquasar was found along with X-rays or ultraviolet light

with capturing material from its companion star and jets. In this astrophysical system, one can observe the twin high-frequency QPOs. For example, for twin peaks in the power spectra, the lower one in the twin high-frequency QPOs is f_L, and the upper one is f_U. It is always found that $f_U : f_L$ has the perfect 3:2 frequency ratio. Up to now, there is still no consensus on which physical mechanism is responsible for the twin high-frequency QPOs. However, these frequencies are correlated with the orbital characteristic frequencies of a test particle (see [8,9] for reviews). In the following section, we investigate the twin high-frequency QPOs for the charged particle, which are modeled as RGISBHs immersed in the external magnetic field.

We assume the charged particle has the stable circular orbit r_0. For small displacements (namely, δr and $\delta\theta$) around the mean orbit, it gives $r = r_0 + \delta r$ and $\theta = \pi/2 + \delta\theta$ at the linear order. When we ignore non-linear coupling effects of the vertical and radial modes, it yields

$$\delta\ddot{r} + \bar{\omega}_r^2 \delta r = 0, \tag{43}$$

$$\delta\ddot{\theta} + \bar{\omega}_\theta^2 \delta\theta = 0, \tag{44}$$

where $\bar{\omega}_\theta$ and $\bar{\omega}_r$ denote vertical and radial epicyclic frequencies measured by the local observer, respectively. $\bar{\omega}_\phi$ is determined by $\dot{\phi}$ (see Equation (40)). These frequencies have

$$\bar{\omega}_r^2 = \frac{1}{g_{rr}} \frac{\partial^2 U(r,\theta,E,L,b)}{\partial r^2}, \tag{45}$$

$$\bar{\omega}_\theta^2 = \frac{1}{g_{\theta\theta}} \frac{\partial^2 U(r,\theta,E,L,b)}{\partial \theta^2}, \tag{46}$$

$$\bar{\omega}_\phi = \frac{1}{g_{\phi\phi}} \left(L - \frac{1}{2} b r^2 \right), \tag{47}$$

measured by the local observer. Then, for a distant observer, the corresponding frequencies ω_r, ω_θ and ω_ϕ can be derived as follows:

$$\omega = \left(\frac{1}{2\pi} \frac{c^3}{GM} \right) \left[\frac{\bar{\omega}}{(-g^{tt})E} \right], \tag{48}$$

where $\bar{\omega}$ is derived by Equations (45)–(47), respectively.

From Equation (48), Figures 9 and 10 display the epicyclic motions for the charged particle around RGISBHs with different parameters λ, γ, and b immersed in the external uniform magnetic field. These figures show the vertical epicyclic frequency ω_θ, the orbital frequency ω_ϕ, and the radial epicyclic frequency ω_r change with r/M. Blue dotted vertical lines denote the positions of the 3:2 resonance between ω_θ and ω_r; brown dotted vertical lines denote the ones between ω_ϕ and ω_r; black dotted vertical lines denote the ones between ω_ϕ and ω_θ. Based on Figures 9 and 10, we explicitly show that the difference between the three frequencies mainly depends on the parameters λ, γ, and b. Obviously, the difference between the frequencies is due to the different position of the ISCOs. It also leads to the 3:2 resonance shift (see Figures 9 and 10).

The ratio of twin high-frequency frequencies (namely, $f_U : f_L = 3 : 2$) has been observed in three microquasar in our galaxy, which are GRO 1655-40, XTE 1550-564, and GRS 1915+105 [149]. We can assume that the upper frequency f_U and the lower frequency f_L in twin high-frequency frequencies are, respectively, ω_θ and ω_r. For other situations, we can also either assume $f_U = \omega_r$ and $f_L = \omega_\phi$ or assume $f_U = \omega_\theta$ and $f_L = \omega_\phi$. The vertical lines in Figures 9 and 10 show these cases. In order to probe some possible quantum effects under RGISBHs on the observations, we plot the effects of the parameters λ and γ on the relations between mass $M/M_\odot$ and the upper frequency f_U (Hz) with respect to the data of three microquasars (see Figure 11). In Figure 11, we take three cases into account, which are $f_U : f_L = \omega_\theta : \omega_r$, $f_U : f_L = \omega_\phi : \omega_r$, and $f_U : f_L = \omega_\phi : \omega_\theta$. GRO 1655-40, XTE 1550-564,

and GRS 1915+105 in Figure 11 are denoted by black horizontal lines. Based on Figure 11, this also suggests that λ and γ in RGISBHs best fit the data of the above observations with a non-vanishing magnetic field. This means that the epicyclic motions of charged particles around RGISBHs in the external magnetic field can give one possible explanation for the 3:2 resonance in three low-mass X-ray binaries.

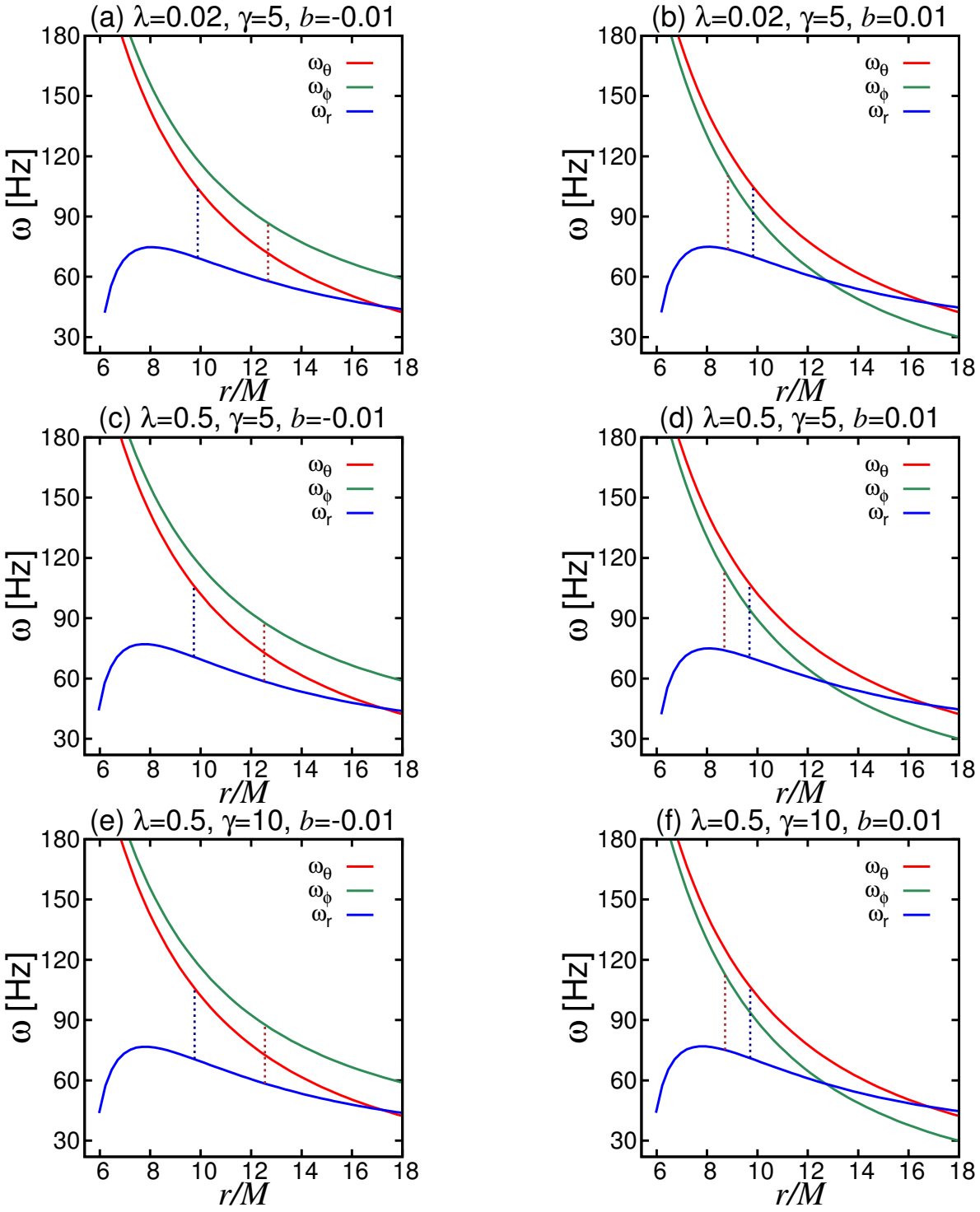

Figure 9. The epicyclic frequencies for RGISBHs immersed in an external uniform magnetic field by taking $M/M_{\odot} = 10$. Blue dotted vertical lines denote the positions of the 3:2 resonance between ω_θ and ω_r and brown dotted vertical lines denote the ones between ω_ϕ and ω_r.

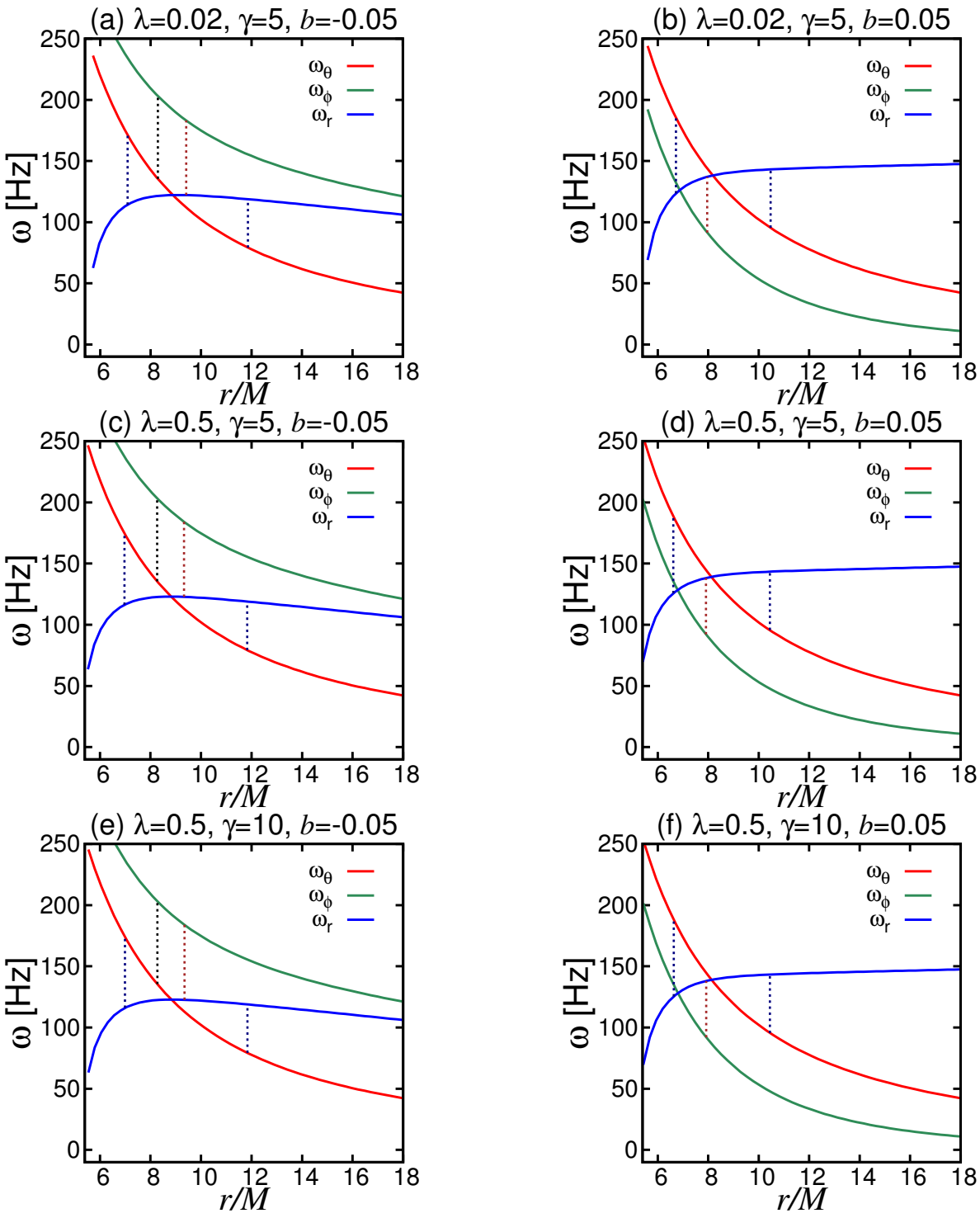

Figure 10. The epicyclic frequencies for RGISBHs immersed in an external uniform magnetic field by taking $M/M_{\odot} = 10$. Blue dotted vertical lines denote the positions of the 3:2 resonance between ω_θ and ω_r; brown dotted vertical lines denote the ones of the 3:2 resonance between ω_ϕ and ω_r; black dotted vertical lines denote the ones between ω_ϕ and ω_θ.

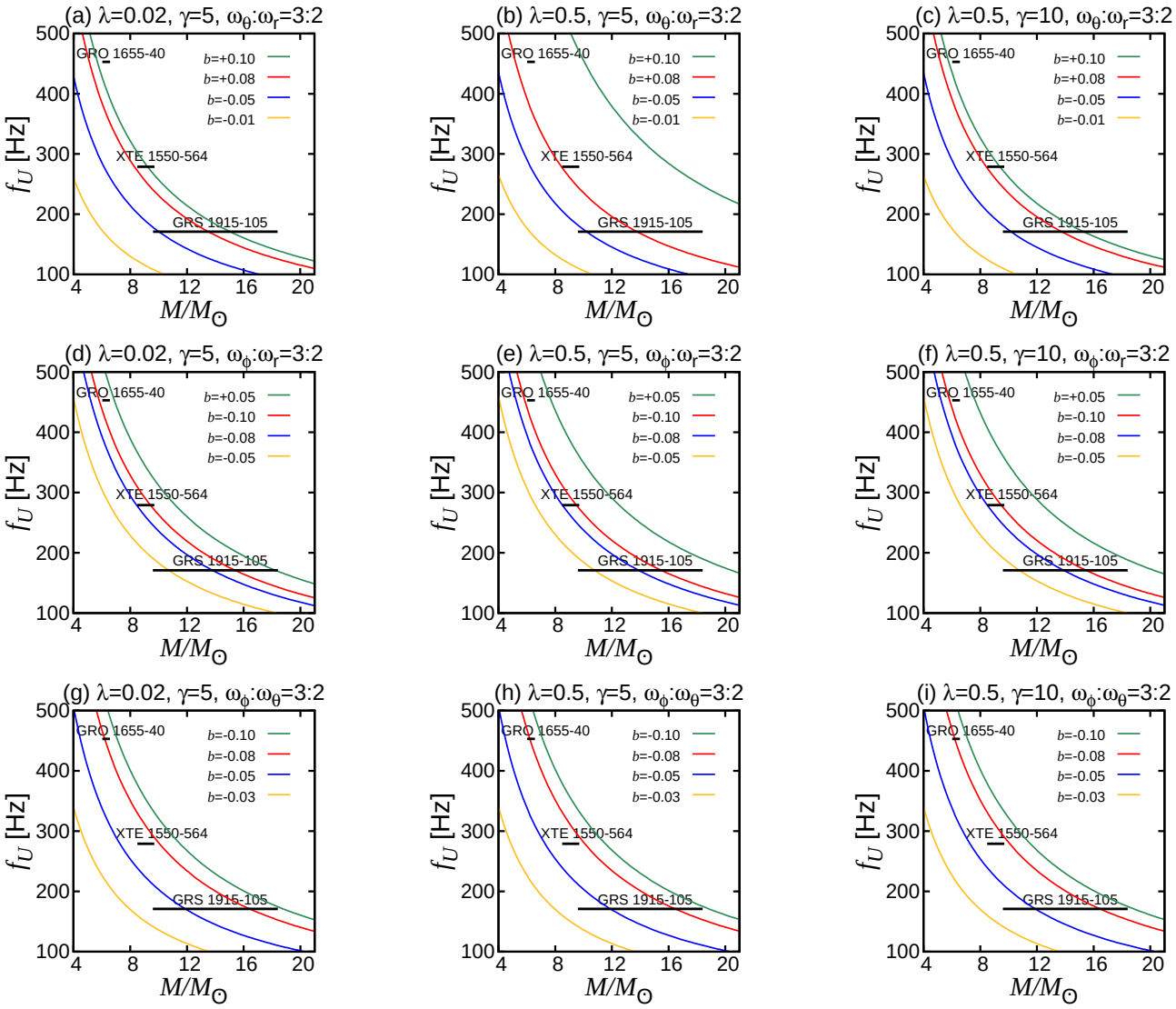

Figure 11. The upper frequency f_U(Hz) and mass $M/M_\odot$ relations for different parameters λ, γ, and b with the cases of $\omega_\theta : \omega_r = 3 : 2$, $\omega_\phi : \omega_r = 3 : 2$, and $\omega_\phi : \omega_\theta = 3 : 2$. GRO 1655-40, XTE 1550-564, and GRS 1915+105 are denoted by black horizontal lines.

6. Conclusions and Discussion

In the present work, we studied timelike particles' bound orbits around renormalization group improved Schwarzschild black holes (RGISBHs), which originate from renormalization group improvement of the Einstein–Hilbert action by using the running Newton constant. By considering the timelike particle's bound orbits between the marginally bound orbits (MBOs) and the innermost stable circular orbits (ISCOs) around RGISBHs, we found that the values for $r_{\rm MBO}/M$, $L_{\rm MBO}/M$, $r_{\rm ISCO}/M$, $L_{\rm ISCO}/M$, and $E_{\rm ISCO}$ are smaller than the values in Schwarzschild black holes in some cases (e.g., $0.25 < \lambda < 1$). Besides, in RGISBHs, the allowed regions of the $(L/M, E)$ for the particle's bound orbits were discussed and analyzed. This indicates that $E_{\rm min} \leq E \leq E_{\rm max}$ for the bound orbits with a fixed L/M.

By considering the secular periastron precession for the timelike particles orbiting around RGISBHs, we obtained $0.6 \leq \gamma \leq 1.02$ when $0.02 \leq \lambda \leq 0.22$ by using the data of GRAVITY. This also suggests that it is not feasible to distinguish such black holes from Schwarzschild ones in the weak gravitational field. Then, in the strong gravitational field, periodic orbits for the particles were investigated by employing a taxonomy. This indicates

that the variation of the parameters in RGISBHs can change the taxonomy. This leads to a transition from periodic motion around Schwarzschild black holes to a quasi-periodic motion around these black holes. After that, the epicyclic motions of charged particles around RGISBHs immersed in an external asymptotically uniform magnetic field were taken into account with respect to the observed twin peak quasi-periodic oscillations' frequencies. The epicyclic motions of charged particles around such black holes in the external magnetic field can give one possible explanation for the 3:2 resonance in three low-mass X-ray binaries: GRS 1915+105, XTE 1550-564, and GRO 1655-40.

Our results might provide some hints to distinguish RGISBHs from the classical black holes by using periodic orbits and epicyclic motions around the strong gravitational field. In the near future observations, if GRAVITY can find S stars nearby Sgr A* and report these precessions in the orbit around Sgr A* with the high-precision, quasi-periodic orbits around RGISBHs, like Figure 8, will be detectable. The quantum gravity effect in epicyclic motions around RGISBHs will also be found only if these observations are modeled under RGISBHs. We leave the detailed investigation on this issue for future works. In this paper, the bound orbits around RGISBHs without spin were investigated. It is well known that the metric with spin will lead to a 3:2 frequency ratio [127]. Another open issue for RGISBHs is hot spots around Sgr A* as magnetized objects, as in the case of [150–152]. This detailed research on the above issues will be considered in our future works.

Author Contributions: H.-Y.L., Methodology, Software, Validation; X.-M.D., Supervision, Conceptualization, Methodology, Software, Writing—original draft. All authors have read and agreed to the published version of the manuscript.

Funding: This work was funded by the National Natural Science Foundation of China (Grant Nos. 12173094, 11773080, and 11473072) and the Strategic Priority Research Program of the Chinese Academy of Sciences (Grant No. XDA15016700).

Data Availability Statement: Our paper is a theoretical work. All of the data in the paper are adopted by the related references.

Conflicts of Interest: The authors declare no conflict of interest.

References

1. LIGO Scientific Collaboration and Virgo Collaboration. Observation of Gravitational Waves from a Binary Black Hole Merger. *Phys. Rev. Lett.* **2016**, *116*, 061102. Available online: http://xxx.lanl.gov/abs/1602.03837 (accessed on 1 January 2022). [CrossRef] [PubMed]
2. LIGO Scientific Collaboration and Virgo Collaboration. Binary Black Hole Mergers in the First Advanced LIGO Observing Run. *Phys. Rev.* **2016**, *6*, 041015. Available online: http://xxx.lanl.gov/abs/1606.04856 (accessed on 1 January 2022). [CrossRef]
3. LIGO Scientific Collaboration and Virgo Collaboration. GW151226: Observation of Gravitational Waves from a 22-Solar-Mass Binary Black Hole Coalescence. *Phys. Rev. Lett.* **2016**, *116*, 241103. Available online: http://xxx.lanl.gov/abs/1606.04855 (accessed on 1 January 2022). [CrossRef]
4. LIGO Scientific Collaboration and Virgo Collaboration. GW170104: Observation of a 50-Solar-Mass Binary Black Hole Coalescence at Redshift 0.2. *Phys. Rev. Lett.* **2017**, *118*, 221101. Available online: http://xxx.lanl.gov/abs/1706.01812 (accessed on 1 January 2022). [CrossRef]
5. LIGO Scientific Collaboration and Virgo Collaboration. GW170608: Observation of a 19 Solar-mass Binary Black Hole Coalescence. *Astrophys. J. Lett.* **2017**, *851*, L35. Available online: http://xxx.lanl.gov/abs/1711.05578 (accessed on 1 January 2022). [CrossRef]
6. LIGO Scientific Collaboration and Virgo Collaboration. GW170814: A Three-Detector Observation of Gravitational Waves from a Binary Black Hole Coalescence. *Phys. Rev. Lett.* **2017**, *119*, 141101. Available online: http://xxx.lanl.gov/abs/1709.09660 (accessed on 1 January 2022). [CrossRef]
7. Webster, B.L.; Murdin, P. Cygnus X-1-a Spectroscopic Binary with a Heavy Companion? *Nature* **1972**, *235*, 37–38. [CrossRef]
8. Bambi, C. *Black Holes: A Laboratory for Testing Strong Gravity*; Springer: Berlin/Heidelberg, Germany, 2017. [CrossRef]
9. Bambi, C. Testing black hole candidates with electromagnetic radiation. *Rev. Mod. Phys.* **2017**, *89*, 025001. Available online: http://xxx.lanl.gov/abs/1509.03884 (accessed on 1 January 2022). [CrossRef]
10. Event Horizon Telescope Collaboration. First M87 Event Horizon Telescope Results. I. The Shadow of the Supermassive Black Hole. *Astrophys. J. Lett.* **2019**, *875*, L1. Available online: http://xxx.lanl.gov/abs/1906.11238 (accessed on 1 January 2022). [CrossRef]
11. Event Horizon Telescope Collaboration. First M87 Event Horizon Telescope Results. II. Array and Instrumentation. *Astrophys. J. Lett.* **2019**, *875*, L2. Available online: http://xxx.lanl.gov/abs/1906.11239 (accessed on 1 January 2022). [CrossRef]

12. Event Horizon Telescope Collaboration. First M87 Event Horizon Telescope Results. III. Data Processing and Calibration. *Astrophys. J. Lett.* **2019**, *875*, L3. Available online: http://xxx.lanl.gov/abs/1906.11240 (accessed on 1 January 2022). [CrossRef]
13. Event Horizon Telescope Collaboration. First M87 Event Horizon Telescope Results. IV. Imaging the Central Supermassive Black Hole. *Astrophys. J. Lett.* **2019**, *875*, L4. Available online: http://xxx.lanl.gov/abs/1906.11241 (accessed on 1 January 2022). [CrossRef]
14. Event Horizon Telescope Collaboration. First M87 Event Horizon Telescope Results. V. Physical Origin of the Asymmetric Ring. *Astrophys. J. Lett.* **2019**, *875*, L5. Available online: http://xxx.lanl.gov/abs/1906.11242 (accessed on 1 January 2022). [CrossRef]
15. Event Horizon Telescope Collaboration. First M87 Event Horizon Telescope Results. VI. The Shadow and Mass of the Central Black Hole. *Astrophys. J. Lett.* **2019**, *875*, L6. Available online: http://xxx.lanl.gov/abs/1906.11243 (accessed on 1 January 2022). [CrossRef]
16. Du, Y.; Tahura, S.; Vaman, D.; Yagi, K. Probing compactified extra dimensions with gravitational waves. *Phys. Rev. D* **2021**, *103*, 044031. Available online: http://xxx.lanl.gov/abs/2004.03051 (accessed on 1 January 2022). [CrossRef]
17. Zulianello, A.; Carballo-Rubio, R.; Liberati, S.; Ansoldi, S. Electromagnetic tests of horizonless rotating black hole mimickers. *Phys. Rev. D* **2021**, *103*, 064071. Available online: http://xxx.lanl.gov/abs/2005.01837 (accessed on 1 January 2022). [CrossRef]
18. Carballo-Rubio, R.; Di Filippo, F.; Liberati, S.; Pacilio, C.; Visser, M. Inner horizon instability and the unstable cores of regular black holes. *J. High Energy Phys.* **2021**, *2021*, 132. Available online: http://xxx.lanl.gov/abs/2101.05006 (accessed on 1 January 2022). [CrossRef]
19. Mazza, J.; Franzin, E.; Liberati, S. A novel family of rotating black hole mimickers. *J. Cosmol. Astropart. Phys.* **2021**, *2021*, 082. Available online: http://xxx.lanl.gov/abs/2102.01105 (accessed on 1 January 2022). [CrossRef]
20. Tsupko, O.Y. Unbound motion of massive particles in the Schwarzschild metric: Analytical description in case of strong deflection. *Phys. Rev. D* **2014**, *89*, 084075. Available online: http://xxx.lanl.gov/abs/1505.06481 (accessed on 1 January 2022). [CrossRef]
21. Jai-akson, P.; Chatrabhuti, A.; Evnin, O.; Lehner, L. Black hole merger estimates in Einstein-Maxwell and Einstein-Maxwell-dilaton gravity. *Phys. Rev. D* **2017**, *96*, 044031. Available online: http://xxx.lanl.gov/abs/1706.06519 (accessed on 1 January 2022). [CrossRef]
22. Levi Said, J.; Mifsud, J.; Parkinson, D.; Saridakis, E.N.; Sultana, J.; Zarb Adami, K. Testing the violation of the equivalence principle in the electromagnetic sector and its consequences in f(T) gravity. *J. Cosmol. Astropart. Phys.* **2020**, *2020*, 47. Available online: http://xxx.lanl.gov/abs/2005.05368 (accessed on 1 January 2022). [CrossRef]
23. Fernandes, P.G.S.; Carrilho, P.; Clifton, T.; Mulryne, D.J. Black holes in the scalar-tensor formulation of 4D Einstein-Gauss-Bonnet gravity: Uniqueness of solutions, and a new candidate for dark matter. *Phys. Rev. D* **2021**, *104*, 044029. [CrossRef]
24. Liu, C.; Zhu, T.; Wu, Q.; Jusufi, K.; Jamil, M.; Azreg-Aïnou, M.; Wang, A. Shadow and quasinormal modes of a rotating loop quantum black hole. *Phys. Rev. D* **2020**, *101*, 084001. Available online: http://xxx.lanl.gov/abs/2003.00477 (accessed on 1 January 2022). [CrossRef]
25. Jusufi, K.; Jamil, M.; Chakrabarty, H.; Wu, Q.; Bambi, C.; Wang, A. Rotating regular black holes in conformal massive gravity. *Phys. Rev. D* **2020**, *101*, 044035. Available online: http://xxx.lanl.gov/abs/1911.07520 (accessed on 1 January 2022). [CrossRef]
26. Abbas, G.; Mahmood, A.; Zubair, M. Strong deflection gravitational lensing for photon coupled to Weyl tensor in a charged Kiselev black hole. *Phys. Dark Univ.* **2021**, *31*, 100750. [CrossRef]
27. Zhou, T.Y.; Cao, W.G.; Xie, Y. Collinear solution to the three-body problem under a scalar-tensor gravity. *Phys. Rev. D* **2016**, *93*, 064065. [CrossRef]
28. Jenks, L.; Yagi, K.; Alexander, S. Probing Noncommutative Gravity with Gravitational Wave and Binary Pulsar Observations. *Phys. Rev. D* **2020**, *102*, 084022. Available online: http://xxx.lanl.gov/abs/2007.09714 (accessed on 1 January 2022). [CrossRef]
29. Izmailov, R.N.; Karimov, R.K.; Potapov, A.A.; Nandi, K.K. String effect on the relative time delay in the Kerr-Sen black hole. *Ann. Phys.* **2020**, *413*, 168069. Available online: http://xxx.lanl.gov/abs/2002.01149 (accessed on 1 January 2022). [CrossRef]
30. Tuleganova, G.Y.; Izmailov, R.N.; Karimov, R.K.; Potapov, A.A.; Nandi, K.K. Times of arrival (TOA) of signals in the Kerr-MOG black hole. *Gen. Relativ. Gravit.* **2020**, *52*, 31. [CrossRef]
31. Caruana, M.; Farrugia, G.; Levi Said, J. Cosmological bouncing solutions in f(T, B) gravity. *Eur. Phys. J. C* **2020**, *80*, 640. Available online: http://xxx.lanl.gov/abs/2007.09925 (accessed on 1 January 2022). [CrossRef]
32. Franco, G.A.R.; Escamilla-Rivera, C.; Levi Said, J. Stability analysis for cosmological models in $f(T, B)$ gravity. *Eur. Phys. J. C* **2020**, *80*, 677. Available online: http://xxx.lanl.gov/abs/2005.14191 (accessed on 1 January 2022). [CrossRef]
33. Carballo-Rubio, R.; Di Filippo, F.; Liberati, S. Hearts of Darkness: The inside out probing of black holes. *arXiv* **2021**, arXiv:2106.01530. Available online: http://xxx.lanl.gov/abs/2106.01530 (accessed on 1 January 2022).
34. Jefremov, P.I.; Tsupko, O.Y.; Bisnovatyi-Kogan, G.S. Innermost stable circular orbits of spinning test particles in Schwarzschild and Kerr space-times. *Phys. Rev. D* **2015**, *91*, 124030. Available online: http://xxx.lanl.gov/abs/1503.07060 (accessed on 1 January 2022). [CrossRef]
35. Favata, M. The gravitational-wave memory from eccentric binaries. *Phys. Rev. D* **2011**, *84*, 124013. Available online: http://xxx.lanl.gov/abs/1108.3121 (accessed on 1 January 2022). [CrossRef]
36. Bambhaniya, P.; Solanki, D.N.; Dey, D.; Joshi, A.B.; Joshi, P.S.; Patel, V. Precession of timelike bound orbits in Kerr spacetime. *Eur. Phys. J. C* **2021**, *81*, 205. Available online: http://xxx.lanl.gov/abs/2007.12086 (accessed on 1 January 2022). [CrossRef]
37. Bambhaniya, P.; Dey, D.; Joshi, A.B.; Joshi, P.S.; Solanki, D.N.; Mehta, A. Shadows and negative precession in non-Kerr spacetime. *Phys. Rev. D* **2021**, *103*, 084005. Available online: http://xxx.lanl.gov/abs/2101.03865 (accessed on 1 January 2022). [CrossRef]

38. Nunes, R.C.; Pan, S.; Saridakis, E.N. New observational constraints on f (T) gravity through gravitational-wave astronomy. *Phys. Rev. D* **2018**, *98*, 104055. Available online: http://xxx.lanl.gov/abs/1810.03942 (accessed on 1 January 2022). [CrossRef]
39. Levi Said, J.; Mifsud, J.; Sultana, J.; Zarb Adami, K. Reconstructing teleparallel gravity with cosmic structure growth and expansion rate data. *J. Cosmol. Astropart. Phys.* **2021**, *2021*, 015, Available online: http://xxx.lanl.gov/abs/2103.05021 (accessed on 1 January 2022). [CrossRef]
40. Lu, X.; Xie, Y. Gravitational lensing by a quantum deformed Schwarzschild black hole. *Eur. Phys. J. C* **2021**, *81*, 627. [CrossRef]
41. Lu, X.; Xie, Y. Time delay of photons coupled to Weyl tensor in a regular phantom black hole. *Eur. Phys. J. C* **2020**, *80*, 625. [CrossRef]
42. Zhang, J.; Xie, Y. Probing a self-complete and Generalized-Uncertainty-Principle black hole with precessing and periodic motion. *Astrophys. Space Sci.* **2022**, *367*, 17. [CrossRef]
43. Zhu, X.Y.; Xie, Y. Strong deflection gravitational lensing by a Lee-Wick ultracompact object. *Eur. Phys. J. C* **2020**, *80*, 444. [CrossRef]
44. Gao, Y.X.; Xie, Y. Gravitational lensing by hairy black holes in Einstein-scalar-Gauss-Bonnet theories. *Phys. Rev. D* **2021**, *103*, 043008. [CrossRef]
45. Gao, Y.X.; Xie, Y. Strong deflection gravitational lensing by an Einstein-Lovelock ultracompact object. *Eur. Phys. J. C* **2022**, *82*, 162. [CrossRef]
46. Cheng, X.T.; Xie, Y. Probing a black-bounce, traversable wormhole with weak deflection gravitational lensing. *Phys. Rev. D* **2021**, *103*, 064040. [CrossRef]
47. Bojowald, M. Loop Quantum Cosmology. *Living Rev. Relativ.* **2005**, *8*, 11. Available online: http://xxx.lanl.gov/abs/gr-qc/0601085 (accessed on 1 January 2022). [CrossRef]
48. Hawking, S.W. Particle creation by black holes. *Commun. Math. Phys.* **1975**, *43*, 199–220. [CrossRef]
49. Bekenstein, J.D.; Mukhanov, V.F. Spectroscopy of the quantum black hole. *Phys. Lett. B* **1995**, *360*, 7–12. Available online: http://xxx.lanl.gov/abs/gr-qc/9505012 (accessed on 1 January 2022). [CrossRef]
50. Hod, S. The Hawking evaporation process of rapidly-rotating black holes: An almost continuous cascade of gravitons. *Eur. Phys. J. C* **2015**, *75*, 329. Available online: http://xxx.lanl.gov/abs/1506.05457 (accessed on 1 January 2022). [CrossRef]
51. Witten, E. Notes on Some Entanglement Properties of Quantum Field Theory. *arXiv* **2018**, arXiv:1803.04993. Available online: http://xxx.lanl.gov/abs/1803.04993 (accessed on 1 January 2022).
52. Faulkner, T.; Guica, M.; Hartman, T.; Myers, R.C.; Van Raamsdonk, M. Gravitation from entanglement in holographic CFTs. *J. High Energy Phys.* **2014**, *2014*, 51. Available online: http://xxx.lanl.gov/abs/1312.7856 (accessed on 1 January 2022). [CrossRef]
53. Almheiri, A.; Marolf, D.; Polchinski, J.; Sully, J. Black holes: Complementarity or firewalls? *J. High Energy Phys.* **2013**, *2013*, 62. Available online: http://xxx.lanl.gov/abs/1207.3123 (accessed on 1 January 2022). [CrossRef]
54. Jefferson, R. Black holes and quantum entanglement. *arXiv* **2019**, arXiv:1901.01149. Available online: http://xxx.lanl.gov/abs/1901.01149 (accessed on 1 January 2022).
55. Hawking, S.W. The Information Paradox for Black Holes. *arXiv* **2015**, arXiv:1509.01147. Available online: http://xxx.lanl.gov/abs/1509.01147 (accessed on 1 January 2022).
56. Gómez, C.; Zell, S. Black hole evaporation, quantum hair and supertranslations. *Eur. Phys. J. C* **2018**, *78*, 320. Available online: http://xxx.lanl.gov/abs/1707.08580 (accessed on 1 January 2022). [CrossRef]
57. Ho, P.M.; Yokokura, Y. Firewall from Effective Field Theory. *Universe* **2021**, *7*, 241. Available online: http://xxx.lanl.gov/abs/2004.04956 (accessed on 1 January 2022). [CrossRef]
58. Cheng, P.; An, Y. Soft black hole information paradox: Page curve from Maxwell soft hair of a black hole. *Phys. Rev. D* **2021**, *103*, 126020. Available online: http://xxx.lanl.gov/abs/2012.14864 (accessed on 1 January 2022). [CrossRef]
59. Contreras, C.; Koch, B.; Rioseco, P. Black hole solution for scale-dependent gravitational couplings and the corresponding coupling flow. *Class. Quantum Gravity* **2013**, *30*, 175009. Available online: http://xxx.lanl.gov/abs/1303.3892 (accessed on 1 January 2022). [CrossRef]
60. Koch, B.; Contreras, C.; Rioseco, P.; Saueressig, F. Black holes and running couplings: A comparison of two complementary approaches. *arXiv* **2013**, arXiv:1311.1121. Available online: http://xxx.lanl.gov/abs/1311.1121 (accessed on 1 January 2022).
61. Koch, B.; Rioseco, P. Black hole solutions for scale-dependent couplings: The de Sitter and the Reissner-Nordström case. *Class. Quantum Gravity* **2016**, *33*, 035002. Available online: http://xxx.lanl.gov/abs/1501.00904 (accessed on 1 January 2022). [CrossRef]
62. Koch, B.; Reyes, I.A.; Rincón, Á. A scale dependent black hole in three-dimensional space-time. *Class. Quantum Gravity* **2016**, *33*, 225010. Available online: http://xxx.lanl.gov/abs/1606.04123 (accessed on 1 January 2022). [CrossRef]
63. Rincón, Á.; Contreras, E.; Bargueño, P.; Koch, B.; Panotopoulos, G.; Hernández-Arboleda, A. Scale-dependent three-dimensional charged black holes in linear and non-linear electrodynamics. *Eur. Phys. J. C* **2017**, *77*, 494. Available online: http://xxx.lanl.gov/abs/1704.04845 (accessed on 1 January 2022). [CrossRef]
64. Rincón, Á.; Panotopoulos, G. Quasinormal modes of scale dependent black holes in (1 + 2)-dimensional Einstein-power-Maxwell theory. *Phys. Rev. D* **2018**, *97*, 024027. Available online: http://xxx.lanl.gov/abs/1801.03248 (accessed on 1 January 2022). [CrossRef]
65. Rincón, Á.; Koch, B. Scale-dependent rotating BTZ black hole. *Eur. Phys. J. C* **2018**, *78*, 1022. Available online: http://xxx.lanl.gov/abs/1806.03024 (accessed on 1 January 2022). [CrossRef]

66. Rincón, Á.; Villanueva, J.R. The Sagnac effect on a scale-dependent rotating BTZ black hole background. *Class. Quantum Gravity* **2020**, *37*, 175003. Available online: http://xxx.lanl.gov/abs/1902.03704 (accessed on 1 January 2022). [CrossRef]
67. Fathi, M.; Rincón, Á.; Villanueva, J.R. Photon trajectories on a first order scale-dependent static BTZ black hole. *Class. Quantum Gravity* **2020**, *37*, 075004 Available online: http://xxx.lanl.gov/abs/1903.09037 (accessed on 1 January 2022). [CrossRef]
68. Rincón, Á.; Panotopoulos, G. Scale-dependent slowly rotating black holes with flat horizon structure. *Phys. Dark Univ.* **2020**, *30*, 100725 Available online: http://xxx.lanl.gov/abs/2009.14678 (accessed on 1 January 2022). [CrossRef]
69. Panotopoulos, G.; Rincón, Á.; Lopes, I. Interior solutions of relativistic stars with anisotropic matter in scale-dependent gravity. *Eur. Phys. J. C* **2021**, *81*, 63 Available online: http://xxx.lanl.gov/abs/2101.06649 (accessed on 1 January 2022). [CrossRef]
70. Panotopoulos, G.; Rincón, Á. Growth of structures and redshift-space distortion data in scale-dependent gravity. *arXiv* **2021**, arXiv:2105.10803. Available online: http://xxx.lanl.gov/abs/2105.10803 (accessed on 1 January 2022).
71. Bonanno, A.; Reuter, M. Renormalization group improved black hole spacetimes. *Phys. Rev. D* **2000**, *62*, 043008. Available online: http://xxx.lanl.gov/abs/hep-th/0002196 (accessed on 1 January 2022). [CrossRef]
72. Bonanno, A.; Reuter, M. Quantum gravity effects near the null black hole singularity. *Phys. Rev. D* **1999**, *60*, 084011. Available online: http://xxx.lanl.gov/abs/gr-qc/9811026 (accessed on 1 January 2022). [CrossRef]
73. Yang, R. Quantum gravity corrections to accretion onto a Schwarzschild black hole. *Phys. Rev. D* **2015**, *92*, 084011. Available online: http://xxx.lanl.gov/abs/1504.04223 (accessed on 1 January 2022). [CrossRef]
74. Lu, X.; Xie, Y. Weak and strong deflection gravitational lensing by a renormalization group improved Schwarzschild black hole. *Eur. Phys. J. C* **2019**, *79*, 1016. [CrossRef]
75. Rayimbaev, J.; Abdujabbarov, A.; Jamil, M.; Ahmedov, B.; H, W.B. Dynamics of test particles around renormalization group improved Schwarzschild black holes. *Phys. Rev. D* **2020**, *102*, 084016. [CrossRef]
76. Will, C.M. *Theory and Experiment in Gravitational Physics*; Cambridge University Press: Cambridge, UK, 1993.
77. Park, R.S.; Folkner, W.M.; Konopliv, A.S.; Williams, J.G.; Smith, D.E.; Zuber, M.T. Precession of Mercury's Perihelion from Ranging to the MESSENGER Spacecraft. *Astron. J.* **2017**, *153*, 121. [CrossRef]
78. Iorio, L.; Saridakis, E.N. Solar system constraints on f(T) gravity. *Mon. Not. R. Astron. Soc.* **2012**, *427*, 1555–1561. Available online: http://xxx.lanl.gov/abs/1203.5781 (accessed on 1 January 2022). [CrossRef]
79. Iorio, L. Constraints on Galileon-induced precessions from solar system orbital motions. *J. Cosmol. Astropart. Phys.* **2012**, *7*, 1. Available online: http://xxx.lanl.gov/abs/1204.0745 (accessed on 1 January 2022). [CrossRef]
80. Xie, Y.; Deng, X.M. f (T) gravity: Effects on astronomical observations and Solar system experiments and upper bounds. *Mon. Not. R. Astron. Soc.* **2013**, *433*, 3584–3589. [CrossRef]
81. Iorio, L. Preliminary bounds of the gravitational local position invariance from Solar system planetary precessions. *Mon. Not. R. Astron. Soc.* **2014**, *437*, 3482–3489. [CrossRef]
82. Ruggiero, M.L.; Radicella, N. Weak-field spherically symmetric solutions in f (T) gravity. *Phys. Rev. D* **2015**, *91*, 104014. Available online: http://xxx.lanl.gov/abs/1501.02198 (accessed on 1 January 2022). [CrossRef]
83. De Martino, I.; Lazkoz, R.; De Laurentis, M. Analysis of the Yukawa gravitational potential in f (R) gravity. I. Semiclassical periastron advance. *Phys. Rev. D* **2018**, *97*, 104067. Available online: http://xxx.lanl.gov/abs/1801.08135 (accessed on 1 January 2022). [CrossRef]
84. Deng, X.M.; Xie, Y. Improved upper bounds on Kaluza-Klein gravity with current Solar System experiments and observations. *Eur. Phys. J. C* **2015**, *75*, 539. Available online: http://xxx.lanl.gov/abs/1510.02946 (accessed on 1 January 2022). [CrossRef]
85. Iorio, L. Classical and relativistic long-term time variations of some observables for transiting exoplanets. *Mon. Not. R. Astron. Soc.* **2011**, *411*, 167–183. Available online: http://xxx.lanl.gov/abs/1007.2780 (accessed on 1 January 2022). [CrossRef]
86. Xie, Y.; Deng, X.M. On the (im)possibility of testing new physics in exoplanets using transit timing variations: Deviation from inverse-square law of gravity. *Mon. Not. R. Astron. Soc.* **2014**, *438*, 1832–1838. Available online: http://xxx.lanl.gov/abs/1401.7407 (accessed on 1 January 2022). [CrossRef]
87. Vargas dos Santos, M.; Mota, D.F. Extrasolar planets as a probe of modified gravity. *Phys. Lett. B* **2017**, *769*, 485–490. Available online: http://xxx.lanl.gov/abs/1603.03243 (accessed on 1 January 2022). [CrossRef]
88. Ruggiero, M.L.; Iorio, L. Probing a r^{-n} modification of the Newtonian potential with exoplanets. *J. Cosmol. Astropart. Phys.* **2020**, *2020*, 042. Available online: http://xxx.lanl.gov/abs/2001.04122 (accessed on 1 January 2022). [CrossRef]
89. Damour, T.; Esposito-Farèse, G. Testing gravity to second post-Newtonian order: A field-theory approach. *Phys. Rev. D* **1996**, *53*, 5541–5578. Available online: http://xxx.lanl.gov/abs/{arXiv:gr-qc/9506063} (accessed on 1 January 2022). [CrossRef]
90. Kramer, M.; Stairs, I.H.; Manchester, R.N.; McLaughlin, M.A.; Lyne, A.G.; Ferdman, R.D.; Burgay, M.; Lorimer, D.R.; Possenti, A.; D'Amico, N.; et al. Tests of General Relativity from Timing the Double Pulsar. *Science* **2006**, *314*, 97–102. Available online: http://xxx.lanl.gov/abs/{arXiv:astro-ph/0609417} (accessed on 1 January 2022). [CrossRef]
91. De Laurentis, M.; De Rosa, R.; Garufi, F.; Milano, L. Testing gravitational theories using eccentric eclipsing detached binaries. *Mon. Not. R. Astron. Soc.* **2012**, *424*, 2371–2379. Available online: http://xxx.lanl.gov/abs/1207.5410 (accessed on 1 January 2022). [CrossRef]
92. De Laurentis, M.; De Martino, I. Testing f (R) theories using the first time derivative of the orbital period of the binary pulsars. *Mon. Not. R. Astron. Soc.* **2013**, *431*, 741–748. Available online: http://xxx.lanl.gov/abs/1302.0220 (accessed on 1 January 2022). [CrossRef]

93. Deng, X.M.; Xie, Y.; Huang, T.Y. Modified scalar-tensor-vector gravity theory and the constraint on its parameters. *Phys. Rev. D* **2009**, *79*, 044014. Available online: http://xxx.lanl.gov/abs/0901.3730 (accessed on 1 January 2022). [CrossRef]
94. Deng, X.M. Solar System and stellar tests of noncommutative spectral geometry. *Eur. Phys. J. Plus* **2017**, *132*, 85. [CrossRef]
95. Hees, A.; Do, T.; Ghez, A.M.; Martinez, G.D.; Naoz, S.; Becklin, E.E.; Boehle, A.; Chappell, S.; Chu, D.; Dehghanfar, A.; et al. Testing General Relativity with Stellar Orbits around the Supermassive Black Hole in Our Galactic Center. *Phys. Rev. Lett.* **2017**, *118*, 211101. Available online: http://xxx.lanl.gov/abs/1705.07902 (accessed on 1 January 2022). [CrossRef] [PubMed]
96. Gravity Collaboration. Detection of the Schwarzschild precession in the orbit of the star S2 near the Galactic centre massive black hole. *Astron. Astrophys.* **2020**, *636*, L5. Available online: http://xxx.lanl.gov/abs/2004.07187 (accessed on 1 January 2022). [CrossRef]
97. De Laurentis, M.; De Martino, I.; Lazkoz, R. Analysis of the Yukawa gravitational potential in f (R) gravity. II. Relativistic periastron advance. *Phys. Rev. D* **2018**, *97*, 104068. Available online: http://xxx.lanl.gov/abs/1801.08136 (accessed on 1 January 2022). [CrossRef]
98. De Laurentis, M.; De Martino, I.; Lazkoz, R. Modified gravity revealed along geodesic tracks. *Eur. Phys. J. C* **2018**, *78*, 916. Available online: http://xxx.lanl.gov/abs/1811.00046 (accessed on 1 January 2022). [CrossRef]
99. Glampedakis, K.; Kennefick, D. Zoom and whirl: Eccentric equatorial orbits around spinning black holes and their evolution under gravitational radiation reaction. *Phys. Rev. D* **2002**, *66*, 044002. Available online: http://xxx.lanl.gov/abs/gr-qc/0203086 (accessed on 1 January 2022). [CrossRef]
100. Barack, L.; Cutler, C. LISA capture sources: Approximate waveforms, signal-to-noise ratios, and parameter estimation accuracy. *Phys. Rev. D* **2004**, *69*, 082005. Available online: http://xxx.lanl.gov/abs/gr-qc/0310125 (accessed on 1 January 2022). [CrossRef]
101. Haas, R. Scalar self-force on eccentric geodesics in Schwarzschild spacetime: A time-domain computation. *Phys. Rev. D* **2007**, *75*, 124011. Available online: http://xxx.lanl.gov/abs/0704.0797 (accessed on 1 January 2022). [CrossRef]
102. Healy, J.; Levin, J.; Shoemaker, D. Zoom-Whirl Orbits in Black Hole Binaries. *Phys. Rev. Lett.* **2009**, *103*, 131101. Available online: http://xxx.lanl.gov/abs/0907.0671 (accessed on 1 January 2022). [CrossRef]
103. Levin, J.; Perez-Giz, G. A periodic table for black hole orbits. *Phys. Rev. D* **2008**, *77*, 103005. Available online: http://xxx.lanl.gov/abs/0802.0459 (accessed on 1 January 2022). [CrossRef]
104. Misra, V.; Levin, J. Rational orbits around charged black holes. *Phys. Rev. D* **2010**, *82*, 083001. Available online: http://xxx.lanl.gov/abs/1007.2699 (accessed on 1 January 2022). [CrossRef]
105. Babar, G.Z.; Babar, A.Z.; Lim, Y.K. Periodic orbits around a spherically symmetric naked singularity. *Phys. Rev. D* **2017**, *96*, 084052. [CrossRef]
106. Bambhaniya, P.; Joshi, A.B.; Dey, D.; Joshi, P.S. Timelike geodesics in naked singularity and black hole spacetimes. *Phys. Rev. D* **2019**, *100*, 124020. Available online: http://xxx.lanl.gov/abs/1908.07171 (accessed on 1 January 2022). [CrossRef]
107. Zhou, T.Y.; Xie, Y. Precessing and periodic motions around a black-bounce/traversable wormhole. *Eur. Phys. J. C* **2020**, *80*, 1070. [CrossRef]
108. Wei, S.W.; Yang, J.; Liu, Y.X. Geodesics and periodic orbits in Kehagias-Sfetsos black holes in deformed Horava-Lifshitz gravity. *Phys. Rev. D* **2019**, *99*, 104016. Available online: http://xxx.lanl.gov/abs/1904.03129 (accessed on 1 January 2022). [CrossRef]
109. Liu, C.Q.; Ding, C.K.; Jing, J.L. Periodic Orbits Around Kerr Sen Black Holes. *Commun. Theor. Phys.* **2019**, *71*, 1461. Available online: http://xxx.lanl.gov/abs/1804.05883 (accessed on 1 January 2022). [CrossRef]
110. Lin, H.Y.; Deng, X.M. Precessing and periodic orbits around Lee-Wick black holes. *Eur. Phys. J. Plus* **2022**, *137*, 176. [CrossRef]
111. Lin, H.Y.; Deng, X.M. Rational orbits around 4 D Einstein-Lovelock black holes. *Phys. Dark Univ.* **2021**, *31*, 100745. [CrossRef]
112. Deng, X.M. Periodic orbits around brane-world black holes. *Eur. Phys. J. C* **2020**, *80*, 489. [CrossRef]
113. Deng, X.M. Geodesics and periodic orbits around quantum-corrected black holes. *Phys. Dark Univ.* **2020**, *30*, 100629. [CrossRef]
114. Gao, B.; Deng, X.M. Bound orbits around modified Hayward black holes. *Mod. Phys. Lett. A* **2021**, *36*, 2150237. [CrossRef]
115. Gao, B.; Deng, X.M. Bound orbits around Bardeen black holes. *Ann. Phys.* **2020**, *418*, 168194. [CrossRef]
116. Bambi, C. Probing the space-time geometry around black hole candidates with the resonance models for high-frequency QPOs and comparison with the continuum-fitting method. *J. Cosmol. Astropart. Phys.* **2012**, *2012*, 014. Available online: http://xxx.lanl.gov/abs/1205.6348 (accessed on 1 January 2022). [CrossRef]
117. Bambi, C.; Nampalliwar, S. Quasi-periodic oscillations as a tool for testing the Kerr metric: A comparison with gravitational waves and iron line. *Europhys. Lett.* **2016**, *116*, 30006. Available online: http://xxx.lanl.gov/abs/1604.02643 (accessed on 1 January 2022). [CrossRef]
118. Bambi, C. Testing the nature of the black hole candidate in GRO J1655-40 with the relativistic precession model. *arXiv* **2013**, arXiv:1312.2228. Available online: http://xxx.lanl.gov/abs/1312.2228 (accessed on 1 January 2022).
119. Aliev, A.N.; Daylan Esmer, G.; Talazan, P. Strong gravity effects of rotating black holes: Quasi-periodic oscillations. *Class. Quantum Gravity* **2013**, *30*, 045010. Available online: http://xxx.lanl.gov/abs/1205.2838 (accessed on 1 January 2022). [CrossRef]
120. Johannsen, T.; Psaltis, D. Testing the No-hair Theorem with Observations in the Electromagnetic Spectrum. III. Quasi-periodic Variability. *Astrophys. J.* **2011**, *726*, 11. Available online: http://xxx.lanl.gov/abs/1010.1000 (accessed on 1 January 2022). [CrossRef]
121. Shaymatov, S.; Vrba, J.; Malafarina, D.; Ahmedov, B.; Stuchlík, Z. Charged particle and epicyclic motions around 4 D Einstein-Gauss-Bonnet black hole immersed in an external magnetic field. *Phys. Dark Univ.* **2020**, *30*, 100648. Available online: http://xxx.lanl.gov/abs/2005.12410 (accessed on 1 January 2022). [CrossRef]

122. Azreg-Aïnou, M.; Chen, Z.; Deng, B.; Jamil, M.; Zhu, T.; Wu, Q.; Lim, Y.K. Orbital mechanics and quasiperiodic oscillation resonances of black holes in Einstein-Æther theory. *Phys. Rev. D* **2020**, *102*, 044028. Available online: http://xxx.lanl.gov/abs/2004.02602 (accessed on 1 January 2022). [CrossRef]
123. Maselli, A.; Gualtieri, L.; Pani, P.; Stella, L.; Ferrari, V. Testing Gravity with Quasi-periodic Oscillations from Accreting Black Holes: The Case of Einstein-Dilaton-Gauss-Bonnet Theory. *Astrophys. J.* **2015**, *801*, 115. Available online: http://xxx.lanl.gov/abs/1412.3473 (accessed on 1 January 2022). [CrossRef]
124. Kološ, M.; Stuchlík, Z.; Tursunov, A. Quasi-harmonic oscillatory motion of charged particles around a Schwarzschild black hole immersed in a uniform magnetic field. *Class. Quantum Gravity* **2015**, *32*, 165009. Available online: http://xxx.lanl.gov/abs/1506.06799 (accessed on 1 January 2022). [CrossRef]
125. Staykov, K.V.; Doneva, D.D.; Yazadjiev, S.S. Orbital and epicyclic frequencies around neutron and strange stars in R^2 gravity. *Eur. Phys. J. C* **2015**, *75*, 607, Available online: http://xxx.lanl.gov/abs/1508.07790 (accessed on 1 January 2022). [CrossRef]
126. Staykov, K.V.; Doneva, D.D.; Yazadjiev, S.S. Orbital and epicyclic frequencies in massive scalar-tensor theory with self-interaction. *Astrophys. Space Sci.* **2019**, *364*, 178. Available online: http://xxx.lanl.gov/abs/1902.09208 (accessed on 1 January 2022). [CrossRef]
127. Ghasemi-Nodehi, M.; Lu, Y.; Chen, J.; Yang, C. Testing Ghasemi-Nodehi-Bambi metric parameters with quasi-periodic oscillations. *Eur. Phys. J. C* **2020**, *80*, 504. Available online: http://xxx.lanl.gov/abs/2006.13638 (accessed on 1 January 2022). [CrossRef]
128. Stuchlík, Z.; Kotrlová, A. Orbital resonances in discs around braneworld Kerr black holes. *Gen. Relativ. Gravit.* **2009**, *41*, 1305–1343. Available online: http://xxx.lanl.gov/abs/0812.5066 (accessed on 1 January 2022). [CrossRef]
129. Hawking, S.W. Gravitational Radiation from Colliding Black Holes. *Phys. Rev. Lett.* **1971**, *26*, 1344–1346. [CrossRef]
130. Rindler, W. *Relativity: Special, General, and Cosmological*, 2nd ed.; Oxford University Press: Oxford, UK, 2006.
131. Misner, C.W.; Thorne, K.S.; Wheeler, J.A. *Gravitation*; Freeman: San Francisco, CA, USA, 1973.
132. Klioner, S.A.; Kopeikin, S.M. The Post-Keplerian Orbital Representations of the Relativistic Two-Body Problem. *Astrophys. J.* **1994**, *427*, 951. [CrossRef]
133. Wald, R.M. Black hole in a uniform magnetic field. *Phys. Rev. D* **1974**, *10*, 1680–1685. [CrossRef]
134. Frolov, V.P.; Shoom, A.A. Motion of charged particles near a weakly magnetized Schwarzschild black hole. *Phys. Rev. D* **2010**, *82*, 084034. Available online: http://xxx.lanl.gov/abs/1008.2985 (accessed on 1 January 2022). [CrossRef]
135. Frolov, V.P.; Krtouš, P. Charged particle in higher dimensional weakly charged rotating black hole spacetime. *Phys. Rev. D* **2011**, *83*, 024016. Available online: http://xxx.lanl.gov/abs/1010.2266 (accessed on 1 January 2022). [CrossRef]
136. Frolov, V.P. Weakly magnetized black holes as particle accelerators. *Phys. Rev. D* **2012**, *85*, 024020. Available online: http://xxx.lanl.gov/abs/1110.6274 (accessed on 1 January 2022). [CrossRef]
137. Kovář, J.; Kopáček, O.; Karas, V.; Stuchlík, Z. Off-equatorial orbits in strong gravitational fields near compact objects—II: halo motion around magnetic compact stars and magnetized black holes. *Class. Quantum Gravity* **2010**, *27*, 135006. Available online: http://xxx.lanl.gov/abs/1005.3270 (accessed on 1 January 2022). [CrossRef]
138. Kovář, J.; Slaný, P.; Cremaschini, C.; Stuchlík, Z.; Karas, V.; Trova, A. Electrically charged matter in rigid rotation around magnetized black hole. *Phys. Rev. D* **2014**, *90*, 044029. Available online: http://xxx.lanl.gov/abs/1409.0418 (accessed on 1 January 2022). [CrossRef]
139. Gao, B.; Deng, X.M. Dynamics of charged test particles around quantum-corrected Schwarzschild black holes. *Eur. Phys. J. C* **2021**, *81*, 983. [CrossRef]
140. Zhou, N.; Zhang, H.; Liu, W.; Wu, X. A Note on the Construction of Explicit Symplectic Integrators for Schwarzschild Spacetimes. *Astrophys. J.* **2022**, *927*, 160. Available online: http://xxx.lanl.gov/abs/2201.02922 (accessed on 1 January 2022). [CrossRef]
141. Wu, X.; Zhang, H. Chaotic Dynamics in a Superposed Weyl Spacetime. *Astrophys. J.* **2006**, *652*, 1466–1474. [CrossRef]
142. Chen, S.; Wang, M.; Jing, J. Chaotic motion of particles in the accelerating and rotating black holes spacetime. *J. High Energy Phys.* **2016**, *2016*, 82. Available online: http://xxx.lanl.gov/abs/1604.02785 (accessed on 1 January 2022). [CrossRef]
143. Wu, X.; Xie, Y. Revisit on "Ruling out chaos in compact binary systems". *Phys. Rev. D* **2007**, *76*, 124004. Available online: http://xxx.lanl.gov/abs/1004.5057 (accessed on 1 January 2022). [CrossRef]
144. Wu, X.; Xie, Y. Resurvey of order and chaos in spinning compact binaries. *Phys. Rev. D* **2008**, *77*, 103012. Available online: http://xxx.lanl.gov/abs/1004.5317 (accessed on 1 January 2022). [CrossRef]
145. Wu, X.; Wang, Y.; Sun, W.; Liu, F. Construction of Explicit Symplectic Integrators in General Relativity. IV. Kerr Black Holes. *Astrophys. J.* **2021**, *914*, 63. Available online: http://xxx.lanl.gov/abs/2106.12356 (accessed on 1 January 2022). [CrossRef]
146. Wang, Y.; Sun, W.; Liu, F.; Wu, X. Construction of Explicit Symplectic Integrators in General Relativity. III. Reissner-Nordström-(anti)-de Sitter Black Holes. *Astrophys. J. Suppl.* **2021**, *254*, 8. Available online: http://xxx.lanl.gov/abs/2103.12272 (accessed on 1 January 2022). [CrossRef]
147. Wang, Y.; Sun, W.; Liu, F.; Wu, X. Construction of Explicit Symplectic Integrators in General Relativity. II. Reissner-Nordström Black Holes. *Astrophys. J.* **2021**, *909*, 22. Available online: http://xxx.lanl.gov/abs/2103.02864 (accessed on 1 January 2022). [CrossRef]
148. Wang, Y.; Sun, W.; Liu, F.; Wu, X. Construction of Explicit Symplectic Integrators in General Relativity. I. Schwarzschild Black Holes. *Astrophys. J.* **2021**, *907*, 66. Available online: http://xxx.lanl.gov/abs/2102.00373 (accessed on 1 January 2022). [CrossRef]
149. Török, G.; Abramowicz, M.A.; Kluźniak, W.; Stuchlík, Z. The orbital resonance model for twin peak kHz quasi periodic oscillations in microquasars. *Astron. Astrophys.* **2005**, *436*, 1–8. [CrossRef]

150. Gravity Collaboration. Detection of orbital motions near the last stable circular orbit of the massive black hole SgrA*. *Astron. Astrophys.* **2018**, *618*, L10. Available online: http://xxx.lanl.gov/abs/1810.12641 (accessed on 1 January 2022). [CrossRef]
151. Tursunov, A.; Zajaček, M.; Eckart, A.; Kološ, M.; Britzen, S.; Stuchlík, Z.; Czerny, B.; Karas, V. Effect of Electromagnetic Interaction on Galactic Center Flare Components. *Astrophys. J.* **2020**, *897*, 99. Available online: http://xxx.lanl.gov/abs/1912.08174 (accessed on 1 January 2022). [CrossRef]
152. Shahzadi, M.; Kološ, M.; Stuchlík, Z.; Habib, Y. Testing alternative theories of gravity by fitting the hot-spot data of Sgr A*. *arXiv* **2022**, arXiv:2201.04442. Available online: http://xxx.lanl.gov/abs/2201.04442 (accessed on 1 January 2022).